Journal of Mathematical Biology
https://doi.org/10.1007/s00285-020-01495-w

Mathematical Biology

A cell–cell repulsion model on a hyperbolic Keller–Segel equation

Xiaoming Fu[1,2] · Quentin Griette[1,2] · Pierre Magal[1,2]

Received: 25 July 2019 / Revised: 13 March 2020

Abstract
In this work, we discuss a cell–cell repulsion model based on a hyperbolic Keller–Segel equation with two populations, which aims at describing the cell growth and dispersion in the co-culture experiment from the work of Pasquier et al. (Biol Direct 6(1):5, 2011). We introduce the notion of solution integrated along the characteristics, which allows us to prove the existence and uniqueness of solutions and the segregation property for the two species. From a numerical perspective, we also observe that our model admits a competitive exclusion principle which is different from the classical competitive exclusion principle for the corresponding ODE model. More importantly, our model shows the complexity of the short term (6 days) co-cultured cell distribution depending on the initial distribution of each species. Through numerical simulations, we show that the impact of the initial distribution on the proportion of each species in the final population lies in the initial number of cell clusters and that the final proportion of each species is not influenced by the precise distribution of the initial distribution. We also find that a fast dispersion rate gives a short-term advantage while the vital dynamics contributes to a long-term population advantage. When the initial condition for the two species is not segregated, the numerical simulations suggest that asymptotic segregation occurs when the dispersion coefficients are not equal for two populations.

Keywords Cell–cell repulsion · Segregation · Hyperbolic PDE

Mathematics Subject Classification 92C17 · 35L60 · 35D30

Xiaoming Fu: The research of this author is supported by China Scholarship Council.

✉ Pierre Magal
pierre.magal@u-bordeaux.fr

1 IMB, UMR 5251, Univ. Bordeaux, 33400 Talence, France

2 IMB, UMR 5251, CNRS, 33400 Talence, France

Published online: 24 April 2020

1 Introduction

In many recent biological experiments, the co-culture of multiple types of cells has been used to improve our understanding of cell–cell interactions. Typical examples of such co-culture experiment include the study of the interaction between cancer cells and normal cells, which plays a crucial role in tumor development, and comparative studies of the resistance of different types of cancer cells to a chemotherapeutic drugs. The goal of this work is to introduce a mathematical model taking into account the growth of the cell population and the physical motion of cells induced by the competition for space in a Petri dish, in order to better understand the spatial segregation between two types of cells and its potential impact on the outcome of co-culture experiments. Such a segregation phenomenon was observed by Pasquier et al. (2012) in a study of protein transfer between two types of human breast cancer cell. Over a 7-day cell co-culture, a spatial competitive exclusion was observed between these two types of cells and a clear boundary was formed between them on day 7 (see Fig. 1). A segregation property in cell co-culture was also studied recently by Taylor et al. (2017), who compared their experimental results with an individual-based model. They found that heterotypic repulsion and homotypic cohesion can account for cell segregation and border formation. A similar segregation property is also found in the mosaic pattern between nections and cadherins in the experiments of Katsunuma et al. (2016).

Early attempts to explain the segregation property by continuum equations date back to 1970s. Shigesada et al. (1979) studied segregation with a nonlinear diffusion model and they found that the spatial segregation acts to stabilize the coexistence of two similar species by relaxing the interspecific competition. Lou and Ni (1996) generalized the model of Shigesada et al and studied the steady state problem for the self/cross-diffusion model. For the nonlinear diffusion model, Bertsch et al. (2012) proved the existence of segregated solutions when the reaction term is of Lotka–Volterra type. Other mechanisms such as nonlocal competition in the framework of the Lotka–Volterra model leading to the segregation are considered in Mimura and Kawasaki (1980), Mimura et al. (1984), Ni et al. (2018). Crooks et al. (2004), Dancer et al. (1999) considered a competition–diffusion system where two populations spatially segregate as the interspecific competition becomes large. Conti et al. (2005) considered a reaction–diffusion system in which asymptotic segregation occurs (the steady states are segregated). One of the main points in the present model is that segregation is achieved directly and not in the asymptotic limit, contrary to Dancer et al. (1999), Crooks et al. (2004) and Conti et al. (2005).

Here instead of using nonlinear diffusion models, we focus on a (hyperbolic) Keller–Segel model. Such models have been used to describe the attraction and repulsion of cell populations when the motion of the cells is driven by the concentration gradient of a chemical substance, a phenomenon known as chemotaxis. Theoretical and mathematical modeling of chemotaxis can be traced back to the pioneering works of Patlak (1953) in the 1950s and Keller and Segel (1971) in the 1970s. It has become an important model in the description of tumor growth or embryonic development. We refer to the review papers of Horstmann (2003) and Hillen and Painter (2009) for a detailed introduction about the Keller–Segel model.

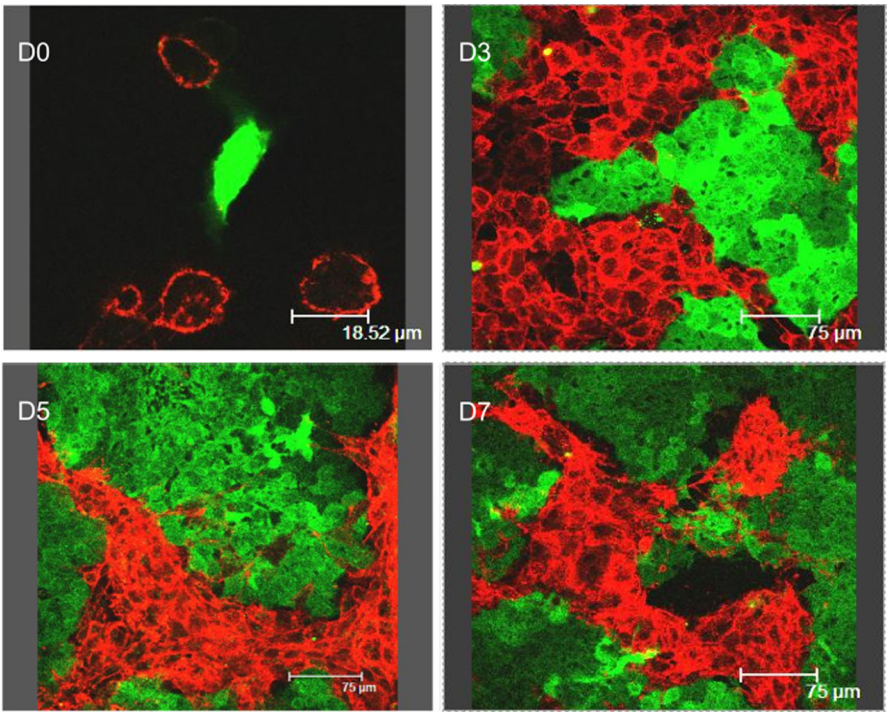

Fig. 1 Direct immunodetection of P-gp transfers in co-cultures of sensitive (MCF-7) and resistant (MCF-7/Doxo) variants of the human breast cancer cell line

As explained in this work, our model can also be regarded as a nonlocal advection model. Recently, implementing nonlocal advection models for the study of cell–cell adhesion and repulsion has attracted a lot of attention. As pointed out by many biologists, cell–cell interactions do not only exist in a local scope, but long-range interactions should also be taken into account to guide the mathematical modeling. Armstrong et al. (2006) in their early work proposed a model (the APS model) in which cells undergo a local diffusion process and a nonlocal advection driven by the adhesion forces, in order to describe cell aggregation and sorting. Based on the APS model, Murakawa and Togashi (2015) thought that the population pressure should come from the cell volume size instead of the linear diffusion, and changed the linear diffusion term into a nonlinear diffusion in order to capture the sharp fronts and the segregation in cell co-culture. Carrillo et al. (2019) recently proposed a new assumption on the adhesion velocity field and their model showed a good agreement with the experiments in the work of Katsunuma et al. (2016). The idea of the long-range attraction and short-range repulsion can also be found in the work of Leverentz et al. (2009). They considered a nonlocal advection model to study the asymptotic behavior of swarms. By choosing a Morse-type kernel which encodes both attractive and repulsive interactions, they found that the solution can asymptotically spread, contract (blow-up), or reach a steady-state. Burger et al. (2014) considered a similar nonlocal adhesion model with nonlinear diffusion. They studied the well-posedness of the model and proved

the existence of a compactly supported, non-constant steady state. Dyson et al. (2010) established the local existence of a classical solution for a nonlocal cell–cell adhesion model in spaces of uniformly continuous functions. For the diffusive model with time delay effect, we refer to Shi et al. (2019a, b) where the authors considered the spatial patterns due to bifurcations. For further Turing and Turing–Hopf bifurcations due to the nonlocal effect, we refer to Ducrot et al. (2018) and Song et al. (2019). We also refer the readers to Mogilner et al. (2003), Eftimie et al. (2007), Ducrot and Magal (2014), Fu and Magal (2018) for more topics about nonlocal advection equations. The derivation of such models as been done in Bellomo et al. (2012) and Morale et al. (2005).

In this work, we consider a two-dimensional bounded domain which represents a flat circular Petri dish. We introduce the notion of solution integrated along the characteristics. Thanks to the appropriate boundary condition of the pressure equation (see Eq. 2.2), we deduce that the characteristics stay in the domain for any positive time. The positivity of solutions, the segregation property and a conservation law follow from the notion of solutions as well. By using numerical simulations, we investigate the impact of the seeding condition (as well as the law of initial distributions) on the proportion of each species in the final population. In the above-mentioned literature, the numerical simulations are restricted to a rectangular domain with periodic boundary conditions. It is worth mentioning that here the domain is circular and the pressure satisfies a no-flux boundary condition (see Appendix 5.4 for numerical scheme).

Our paper is organized as follows. In Sect. 2, we present the model for the single-species case and we prove the local existence and uniqueness of solutions as well as the conservation law by considering the solution integrated along the characteristics. In Sect. 3, we apply our nonlocal advection model established in Sect. 2 to study the cell co-culture. The main goal in this work is to investigate the complexity of the short-term (6 days) co-cultured cell distribution depending on the initial distribution of each species. In Sect. 3.1, we investigate the competitive exclusion principle in our model and compare our spatial model to an ODE model which is homogeneous in space and has been previously studied by Zeeman (1995). In Sect. 3.2, we investigated the impact of the initial distribution on the proportion of each species in the final population. The spatial competition due to the dispersion coefficients and cell kinetics is considered in Sect. 3.3. Section 4 is devoted to discussion and conclusion. We also discuss the case of overlapping (non-segregated) initial conditions for the two species, and how numerical simulations suggest that asymptotic segregation occurs.

2 Mathematical modeling

2.1 Single species model

Let us consider the following model with one species

$$\begin{cases} \partial_t u(t,x) - d \operatorname{div}\left(u(t,x)\nabla P(t,x)\right) = u(t,x)h(u(t,x)) & \text{in } (0,T]\times\Omega, \\ u(0,x) = u_0(x) & \text{on } \overline{\Omega}, \end{cases} \tag{2.1}$$

where P satisfies the following elliptic equation

$$\begin{cases} (I - \chi\Delta)P(t,x) = u(t,x) & \text{in } (0,T]\times\Omega \\ \nabla P(t,x)\cdot\nu(x) = 0 & \text{on } [0,T]\times\partial\Omega, \end{cases} \tag{2.2}$$

We let $\Omega \subset \mathbb{R}^2$ be the unit open disk centered at $\mathbf{0} = (0,0)$ with radius $r = 1$, i.e., $\Omega = B_{\mathbb{R}^2}(\mathbf{0}, 1)$. Here ν is the outward normal unit vector, d is the dispersion coefficient, χ is the sensing coefficient. The divergence, gradient and Laplacian are taken with respect to x. System (2.1)–(2.2) can be regarded as a hyperbolic Keller–Segel equation (with chemotactic repulsion) on a bounded domain.

Remark 2.1 Equation (2.2) can be derived from the following parabolic equation (which is the classical case in the Keller–Segel equation Horstmann 2003) as ε goes to 0:

$$\varepsilon\partial_t P(t,x) = \chi\Delta P(t,x) + u(t,x) - P(t,x). \tag{2.3}$$

The process of letting $\varepsilon \to 0$ corresponds to the assumption that the dynamics of the chemorepellent is fast compared to the evolution of the cell density. In the case of chemoattractant a variant of such a model was considered by Perthame and Dalibard (2009), Calvez and Dolak-Struß (2008).

Remark 2.2 As we mentioned in the introduction, Eq. (2.2) can be regarded as a non-local integral equation by using the following representation

$$P(t,x) = \int_\Omega \kappa(x,y)u(t,y)dy,$$

where κ is the Green function of the operator $(I - \chi\Delta)^{-1}$ with Neumann boundary conditions.

2.1.1 The invariance of domain Ω and the well-posedness of the model

Note that in System (2.1)–(2.2) we do not impose any boundary condition directly on u. Instead, the boundary condition here is induced by $\nabla P\cdot\nu = 0$. If we consider the associated characteristics flow of (2.1)–(2.2)

$$\begin{cases} \frac{\partial}{\partial t}\Pi(t,s;x) = -d\,\nabla P(t,\Pi(t,s;x)) \\ \Pi(s,s;x) = x \in \Omega, \end{cases} \tag{2.4}$$

where $\Pi(t,s;x)$ is the solution of the non-autonomous ODE, t represents the time variable, s is the initial time and x is the initial position. $\Pi(s,s;x) = x$ is our initial condition. We can prove (see Appendix 5.1) that the characteristics can not leave the domain Ω (see Fig. 2 for an illustration). In fact, we can prove that for any $t > 0$, the mapping $x \mapsto \Pi(t,0;x)$ is a bijection from Ω to itself (see Lemma 2.10). We consider the solution along the characteristics

$$w(t,x) := u(t,\Pi(t,0;x)) \quad x\in\Omega, t > 0.$$

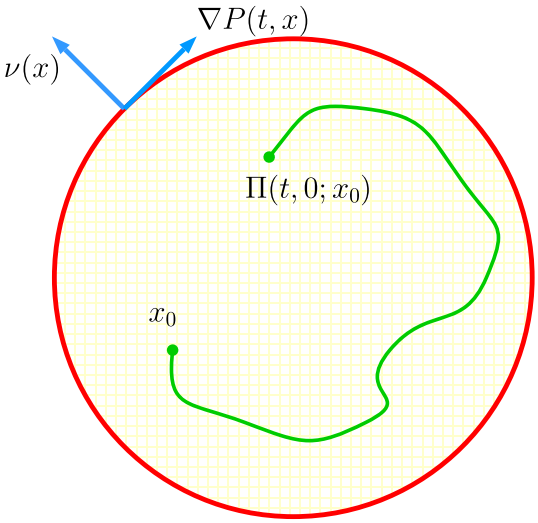

Fig. 2 An illustration of the invariance of the domain Ω. The green curve represents the trajectory of a characteristic (color figure online)

Taking any $x \in \Omega$, there exists $y \in \Omega$ such that $x = \Pi(t, 0; y)$, and since

$$w(t, y) = w(t, \Pi(0, t; x)) = u(t, x),$$

we can reconstruct the solution $u(t, \cdot)$ from the knowledge of $w(t, \cdot)$ and $\{\Pi(t, s, \cdot)\}_{t,s\in[0,T]}$ on Ω.

Assumption 2.3 *The vector field $(t, x) \mapsto \nabla P(t, x)$ is continuous in $[0, T] \times \overline{\Omega}$ and Lipschitz continuous with respect to $x \in \overline{\Omega}$ for each fixed $t \in [0, T]$.*

Remark 2.4 Assumption 2.3 is a sufficient condition for the existence and uniqueness of the characteristic flow $\{\Pi(t, s; \cdot)\}_{t,s\in[0,T]}$ in (2.4).

Definition 2.5 (Evans 1998, Section 5.1) Let $\Omega \subset \mathbb{R}^2$ be a bounded domain. If $u : \Omega \to \mathbb{R}$ is bounded and continuous, we write

$$\|u\|_{C(\overline{\Omega})} := \sup_{x\in\Omega} |u(x)|.$$

For any $\gamma \in (0, 1]$, the γth-Hölder norm of $u : \Omega \to \mathbb{R}$ is

$$\|u\|_{C^{0,\gamma}(\overline{\Omega})} := \|u\|_{C(\overline{\Omega})} + [u]_{C^{0,\gamma}(\overline{\Omega})},$$

where

$$[u]_{C^{0,\gamma}(\overline{\Omega})} := \sup_{\substack{x,y\in\Omega \\ x\neq y}} \left\{ \frac{|u(x) - u(y)|}{|x - y|^{\gamma}} \right\}.$$

The Hölder space $C^{k,\gamma}(\overline{\Omega})$ consists of all functions $u \in C^k(\overline{\Omega})$ having a finite norm

$$\|u\|_{C^{k,\gamma}(\overline{\Omega})} := \sum_{|\alpha|\le k} \|D^\alpha u\|_{C(\overline{\Omega})} + \sum_{|\alpha|=k} [D^\alpha u]_{C^{0,\gamma}(\overline{\Omega})}$$

where $\alpha = (\alpha_1, \dots, \alpha_n) \in \mathbb{N}^n$ and $|\alpha| = \alpha_1 + \cdots + \alpha_n$ in the sum above.

Lemma 2.6 (Gilbarg and Trudinger 2001, Theorem 6.30 and 6.31) *Let $\Omega \subset \mathbb{R}^2$ be the unit open disk. Consider the following elliptic equation*

$$\begin{cases} (I - \chi\Delta)P(x) = u(x) & x \in \Omega, \\ \nabla P(x) \cdot \nu(x) = 0 & x \in \partial\Omega, \end{cases} \tag{2.5}$$

where ν is the outward unit normal vector on $\partial\Omega$. Then for all $u \in C^{0,\alpha}(\overline{\Omega})$, the elliptic problem (2.5) has a unique solution $P \in C^{2,\alpha}(\overline{\Omega})$. Moreover,

$$\|P\|_{C^{2,\alpha}(\overline{\Omega})} \le C\|u\|_{C^{0,\alpha}(\overline{\Omega})},$$

where $C = C(\alpha, \chi, \Omega)$.

The following theorem tells us if we choose our initial value u_0 sufficiently smooth, then Assumption 2.3 is automatically satisfied and the existence and uniqueness of solutions follow.

Theorem 2.7 (Existence and uniqueness of solutions) *Let $u_0 \in W^{1,\infty}(\Omega) \cap C^0_+(\overline{\Omega})$. There exists $T > 0$ such that problem (2.1)–(2.2) has a unique solution $u \in C\left([0,T]; C^0_+(\overline{\Omega})\right)$ which satisfies $u(0,x) = u_0(x)$. Moreover u is non-negative and for any $t \in [0,T]$, we have $u(t,\cdot) \in W^{1,\infty}(\Omega)$ and $\sup_{t\in[0,T]} \|u(t,\cdot)\|_{W^{1,\infty}(\Omega)} < \infty$.*

The proof of Theorem 2.7 will be detailed in Appendix 5.2.

Remark 2.8 Since for any $t \in [0,T]$ and for any $\alpha \in (0,1)$, we have $u(t,\cdot) \in W^{1,\infty}(\Omega) \hookrightarrow C^{0,\alpha}(\overline{\Omega})$, we deduce from Lemma 2.6 that $P(t,\cdot) \in C^{2,\alpha}(\overline{\Omega})$. Therefore, $(t,x) \to \nabla P(t,x)$ is continuous (since $P \in C([0,T]; C^1(\overline{\Omega}))$) and Lipschitz continuous with respect to x which implies that Assumption 2.3 is satisfied.

2.1.2 Conservation law on a volume

If the reaction term $h \equiv 0$ is null in System (2.1)–(2.2), we have a conservation law for u. This can be seen by integrating the solution along the characteristics. In fact, we have the following conservation law.

Theorem 2.9 *For each volume $A \subset \Omega$ and each $0 \le s \le t$ we have*

$$\int_{\Pi(t,s;A)} u(t,x)\mathrm{d}x = \int_A \exp\left(\int_s^t h\left(u\left(l, \Pi(l,s;z)\right)\right)\mathrm{d}l\right) u(s,z)\mathrm{d}z.$$

In particular, if there is no reaction $h = 0$, then for any $0 \le s \le t$

$$\int_{\Pi(t,s;A)} u(t,x)\mathrm{d}x = \int_A u(s,z)\mathrm{d}z.$$

This means that the total number of cells in the volume A is constant along the volumes $\Pi(t,s;A)$.

Before proving Theorem 2.9, we need the following lemma.

Lemma 2.10 *Let $T > 0$ and $\{\Pi(t,s;x)\}_{t,s\in[0,T]}$ be the characteristic flow generated by (2.4). Then the map $x \mapsto \Pi(t,s;x)$ is continuously differentiable and the determinant of the Jacobian matrix is given by*

$$\det J_\Pi(t,s;x) = \exp\left(\int_s^t \frac{d}{\chi}\left(u(l,\Pi(l,s;x)) - P(l,\Pi(l,s;x))\right)\mathrm{d}l\right), \tag{2.6}$$

where $J_\Pi(t,s;x)$ is the Jacobian matrix of $\Pi(t,s;x)$ with respect to x at $(t,s;x)$.

Proof From Theorem 2.7 and Remark 2.8, the mapping $(t,x) \to P(t,x)$ is $C([0,T];C^1(\overline{\Omega}))$ and $P(t,\cdot) \in C^{2,\alpha}(\overline{\Omega})$ for any $\alpha \in (0,1)$ if $u_0 \in W^{1,\infty}(\Omega)$. This ensures that the characteristics $x \to \Pi(t,s;x)$ is continuously differentiable. Taking the partial derivative of Eq. (2.4) with respect to x yields

$$\begin{cases} \partial_t J_\Pi(t,s;x) = -d\, J_{\nabla P}(t,\Pi(t,s;x))J_\Pi(t,s;x) \\ J_\Pi(s,s;x) = \mathrm{Id}, \end{cases}$$

where $J_{\nabla P}(t,\Pi(t,s;x))$ is the Jacobian matrix of $\nabla P(t,x)$ with respect to x at point $(t,\Pi(t,s;x))$. For any matrix-valued C^1 function $A : t \mapsto A(t)$, the Jacobian formula reads as follows

$$\frac{\mathrm{d}}{\mathrm{d}t}\det A(t) = \det A(t) \times \mathrm{Trace}\left(A^{-1}(t)\frac{d}{dt}A(t)\right).$$

Hence, we obtain

$$\begin{aligned} \frac{\mathrm{d}}{\mathrm{d}t}\det J_\Pi(t,s;x) &= \det J_\Pi(t,s;x) \times \mathrm{Trace}\left(J_\Pi(t,s;x)^{-1}J_{\nabla P}(t,\Pi(t,s;x))J_\Pi(t,s;x)\right) \\ &= \det J_\Pi(t,s;x) \times \mathrm{Trace}\left(J_{\nabla P}(t,\Pi(t,s;x))\right) \end{aligned}$$

and since $\mathrm{Trace}\left(J_{\nabla P}(t,\Pi(t,s;x))\right) = (\Delta P)(t,\Pi(t,s;x)) = -\frac{1}{\chi}\left(u(t,\Pi(t,s;x)) - P(t,\Pi(t,s;x))\right)$, we conclude

$$\begin{cases} \dfrac{\mathrm{d}}{\mathrm{d}t}\det J_\Pi(t,s;x) = \det J_\Pi(t,s;x) \times \dfrac{d}{\chi}\left[u(t,\Pi(t,s;x)) - P(t,\Pi(t,s;x))\right] \\ \det J_\Pi(s,s;x) = 1. \end{cases}$$

The result follows. □

Proof Let $\{\Pi(t,s;x)\}_{t,s\in[0,T]}$ to be the characteristic flow generated by (2.4). Given any measurable set $A \subset \Omega$ and any $0 \le s \le t$, we integrate $u(t,x)$ over the volume $\Pi(t,s;A)$ with respect to x

$$\int_\Omega \mathbb{1}_{\Pi(t,s;A)}(x)u(t,x)\mathrm{d}x = \int_\Omega \mathbb{1}_A(z)u(t,\Pi(t,s;z))\det J_\Pi(t,s;z)\mathrm{d}z, \tag{2.7}$$

where we have changed the variable x to $\Pi(t,s;z)$ on the right-hand-side.

We will prove in (5.5) in Appendix 5.2 that

$$\begin{aligned} &u(t,\Pi(t,s;z)) \\ &= u(s,z)\exp\left(\int_s^t h(u(l,\Pi(l,s;z))) + \frac{d}{\chi}\left(P(l,\Pi(l,s;z)) - u(l,\Pi(l,s;z))\right)\mathrm{d}l\right). \end{aligned}$$

Combined with (2.6), this equality yields

$$u(t,\Pi(t,s;z))\det J_\Pi(t,s;z) = u(s,z)\exp\left(\int_s^t h(u(l,\Pi(l,s;z)))\mathrm{d}l\right),$$

and substituting into (2.7) we get

$$\int_\Omega \mathbb{1}_{\Pi(t,s;A)}(x)u(t,x)\mathrm{d}x = \int_\Omega \mathbb{1}_A(z)u(s,z)\exp\left(\int_s^t h(u(l,\Pi(l,s;z)))\mathrm{d}l\right)\mathrm{d}z,$$

which is equivalent to

$$\int_{\Pi(t,s;A)} u(t,x)\mathrm{d}x = \int_A \exp\left(\int_s^t h\left(u\left(l,\Pi(l,s;z)\right)\right)\mathrm{d}l\right)u(s,z)\mathrm{d}z.$$

The result follows. □

Remark 2.11 For the PDE with logistic source, the nonlocal advection term $\mathrm{div}(u(t,x)\nabla P(t,x))$ makes the uniqueness of the equilibrium non-trivial. In our case, the semi-flow associated to the solution is not monotone. Therefore, comparison arguments fail and more complex dynamical behaviors may occur. However, from numerical simulations for the single species model with logistic source $uh(u) = u(b-au)$, we observe that the solution converges to the constant equilibrium of the corresponding ODE case. Let us consider a single species one-dimensional model

$$\begin{aligned} \partial_t u(t,x) - \mathrm{div}(u(t,x)\nabla P(t,x)) &= u(t,x)(1-u(t,x)) \\ (I-\Delta)P(t,x) &= u(t,x), \end{aligned} \qquad [0,T]\times[-1,1]$$

with Neumann boundary conditions $\nabla P\cdot\nu = 0$ for $(t,x)\in[0,T]\times\{-1,1\}$. The behavior of the solution is illustrated in Fig. 3 by using a compactly supported initial condition.

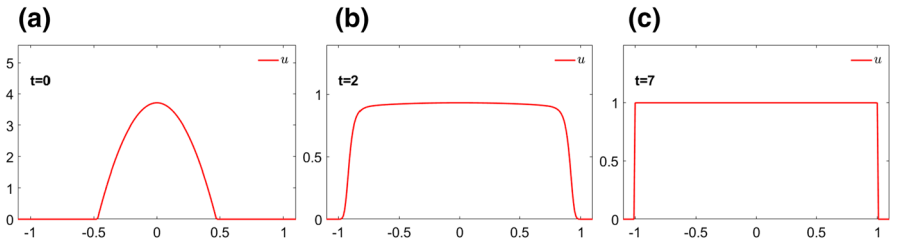

Fig. 3 In this simulation we show that the solution converges numerically to the constant positive steady state

2.2 Multi-species model

2.2.1 Multi-species ODE model

Let us consider the corresponding two species model without the spatial variable x that is $u_i = u_i(t)$ for $i = 1, 2$.

$$\begin{cases} \dfrac{\mathrm{d}u_i}{\mathrm{d}t} = u_i h_i(u_1, u_2) \quad i = 1, 2, \\ u_i(0) = u_{i,0} \in \mathbb{R}_+. \end{cases} \tag{2.8}$$

We adopt the Lotka–Volterra model by setting

$$h_i(u_1, u_2) = b_i - \delta_i - \sum_{j=1}^{2} a_{ij} u_j, \quad i = 1, 2, \tag{2.9}$$

where $b_i > 0$, $i = 1, 2$ are the growth rates, $a_{ij} \geq 0$, $i \neq j$ represent the interspecific competition between the species, a_{ii} is the intraspecific competition (the competition of individuals from the same species) and δ_i is the additional mortality rate caused by drug treatment. In Sect. 2.2.1 we will always assume $\delta_i = 0$ for $i = 1, 2$ without loss of generality (replacing $b_i - \delta_i$ by b_i if $\delta_i > 0$). If we consider (2.8) in the absence of the other species, we can rewrite (2.9) as

$$h_i(u_1, u_2) = b_i - a_{ii} u_i, \quad i = 1, 2.$$

We always assume that for each i, $a_{ii} > 0$ meaning that each species alone exhibits logistic growth. This model has been considered by many authors (for example, see Murray 2003; Zeeman 1995). Here we give a short summary of some qualitative properties of the solution to (2.8) in order to compare it with the PDE model.

Equilibrium and stability for (2.8)–(2.9)

The system has the following equilibria

$$E_0 = (0, 0), \quad E_1 = (P_1, 0), \quad E_2 = (0, P_2), \quad E^* = (u_1^*, u_2^*),$$

where

$$P_1 := \frac{b_1}{a_{11}}, \quad P_2 := \frac{b_2}{a_{22}}, \quad E^* = \left(\frac{a_{22}b_1 - a_{12}b_2}{a_{11}a_{22} - a_{12}a_{21}}, \frac{a_{21}b_1 - a_{11}b_2}{a_{12}a_{21} - a_{11}a_{22}} \right). \quad (2.10)$$

The solution E^* is only of relevance when $a_{12}a_{21} \neq a_{11}a_{22}$ and (u_1^*, u_2^*) is strictly positive, which is equivalent to either condition

$$\begin{cases} \frac{a_{12}}{a_{11}} > \frac{P_1}{P_2} \\ \frac{a_{21}}{a_{22}} > \frac{P_2}{P_1} \end{cases} \quad \text{or} \quad \begin{cases} \frac{a_{12}}{a_{11}} < \frac{P_1}{P_2} \\ \frac{a_{21}}{a_{22}} < \frac{P_2}{P_1}. \end{cases}$$

We adapt the main stability results from Zeeman (1995) where the author considered a general n-species extinction case, Murray (2003, Chapter 3.5) and Hirsch (2012, Chapter 11) to system (2.8)–(2.9) for the following fours cases (i)–(iv) and discuss their biological implications.

Proposition 2.12 *For system (2.8)–(2.9), suppose for each $i = 1, 2$, $b_i > 0, a_{ii} > 0$ and $a_{ij} \geq 0$ for any $i \neq j$. Let $P_1 = b_1/a_{11}$, $P_2 = b_2/a_{22}$ be the equilibrium for each species alone and assume the initial value $(u_{1,0}, u_{2,0})$ lies strictly in the first quadrant that is $u_{1,0} > 0$ and $u_{2,0} > 0$. Then for the following four cases we have*

(i) *$a_{12}/a_{11} < P_1/P_2$, $a_{21}/a_{22} < P_2/P_1$. This case corresponds to Fig. 4a. The system (2.8) has four positive equilibrium, namely E_0, E_1, E_2 and E^*. In such case, only E^* is globally asymptotically stable in the region $\{(u_1, u_2) \in \mathbb{R}^2 \mid u_1 > 0, u_2 > 0\}$.*

(ii) *$a_{12}/a_{11} > P_1/P_2, a_{21}/a_{22} < P_2/P_1$. This case corresponds to Fig. 4b. The system (2.8) has three positive equilibrium, namely E_0, E_1 and E_2. Only E_2 is globally stable in the positive quadrant excepted for the axis $u_1 = 0$.*

(iii) *$a_{12}/a_{11} < P_1/P_2, a_{21}/a_{22} > P_2/P_1$. This case corresponds to Fig. 4c. The analysis of the stability is similar to the case (ii). Only E_1 is globally stable in the positive quadrant excepted for the axis $u_2 = 0$.*

(iv) *$a_{12}/a_{11} > P_1/P_2, a_{21}/a_{22} > P_2/P_1$. This case corresponds to Fig. 4d. In this case, system (2.8) has four equilibrium, where E_1 and E_2 are stable while E^* is a saddle point. The steady states E_1 and E_2 have two non-overlapping domains of attraction, separated by the stable manifold $\boldsymbol{S}$ of the equilibrium E^*.*

Remark 2.13 Although among the four cases, (ii) and (iii) always lead to a competitive exclusion principle and so do (iv) due to the natural perturbation in population levels, case (i) leads to the stable coexistence of the two species in the long term. As we further develop our PDE model for (2.8), we can show numerically that the competitive exclusion principle occurs even in the case (i). This situation is a major difference between the PDE and the ODE model (2.8).

A scheme of the qualitative behavior of the phase trajectory is given in Fig. 4 by numerical simulations.

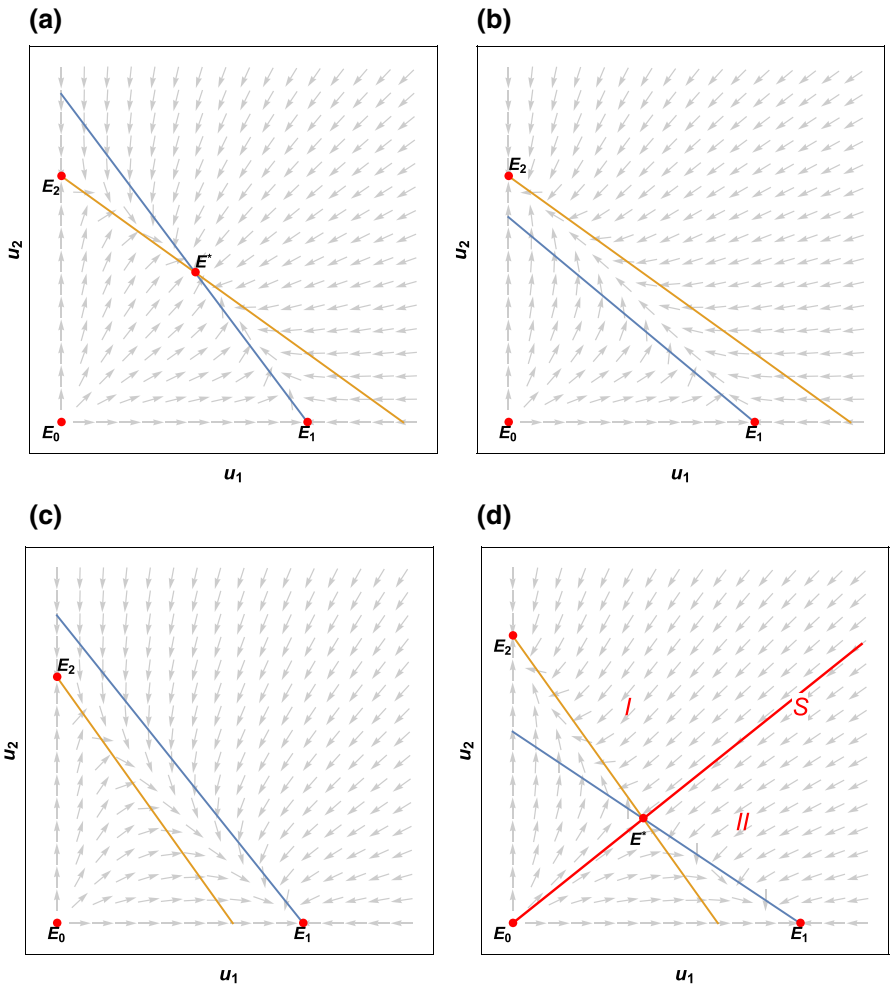

Fig. 4 A scheme of the qualitative behavior of the phase trajectory for various cases. **a** $a_{12}/a_{11} < P_1/P_2$, $a_{21}/a_{22} < P_2/P_1$. Only the positive steady state E^* is stable and all trajectories tend to it. **b** $a_{12}/a_{11} > P_1/P_2, a_{21}/a_{22} < P_2/P_1$. Only one stable steady state E_2 exists with the whole positive quadrant its domain of attraction. **c** $a_{12}/a_{11} < P_1/P_2, a_{21}/a_{22} > P_2/P_1$. Only one stable steady state E_1 exists with the whole positive quadrant its domain of attraction. **d** $a_{12}/a_{11} > P_1/P_2, a_{21}/a_{22} > P_2/P_1$. E_1 and E_2 are stable steady states, each of which has a domain of attraction namely **I** and **II**, separated by a separatrix **S** which is the stable manifold of equilibria E^*

2.2.2 Multi-species PDE model

We study a two species population dynamics model on the unit open disk $\Omega \subset \mathbb{R}^2$ given as follows

$$\begin{cases} \partial_t u_1(t,x) - d_1 \operatorname{div}\big(u_1(t,x)\nabla P(t,x)\big) = u_1(t,x)h_1((u_1,u_2)(t,x)) \\ \partial_t u_2(t,x) - d_2 \operatorname{div}\big(u_2(t,x)\nabla P(t,x)\big) = u_2(t,x)h_2((u_1,u_2)(t,x)) & \text{in } [0,T]\times\Omega, \\ \big(I-\chi\Delta\big)P(t,x) = u_1(t,x)+u_2(t,x) \\ \nabla P(t,x)\cdot\nu(x) = 0 & \text{on } [0,T)\times\partial\Omega, \end{cases} \tag{2.11}$$

where ν is the outward normal vector, d_i is the dispersion coefficient, χ is the sensing coefficient. Recall that the function h_i is given by

$$h_i(u_1,u_2) = b_i - \delta_i - \sum_{j=1}^{2} a_{ij}u_j, \quad i=1,2.$$

System (2.11) is supplemented with the initial condition

$$\mathbf{u}_0(\cdot) := (u_1(0,\cdot), u_2(0,\cdot)) \in C^1(\overline{\Omega})^2. \tag{2.12}$$

2.2.3 Segregation property

It has been observed in mono-layer co-culture experiments that once the two cell populations confront each other, they will stop growing, thus, forming separated islets. We can prove that our model (2.11) preserves such segregation property.

Theorem 2.14 *Suppose* $\mathbf{u} = (u_1,u_2)(t,x)$ *is the solution of* (2.11)–(2.12) *and assume* $d_1 = d_2 = d$ *in* (2.11). *Then for any initial distribution with* $u_1(0,x)u_2(0,x) = 0$ *for all* $x\in\Omega$, *we have* $u_1(t,x)u_2(t,x) = 0$ *for any* $t>0$ *and* $x\in\Omega$.

Proof We argue by contradiction and assume that there exist $t^*>0, x^*\in\Omega$ such that

$$u_1(t^*,x^*)u_2(t^*,x^*) > 0.$$

Recall that the characteristic flow satisfies the following equation

$$\begin{cases} \frac{\partial}{\partial t}\Pi(t,s;x) = -d\,\nabla P(t,\Pi(t,s;x)) \\ \Pi(s,s;x) = x\in\Omega. \end{cases}$$

Since $x\to\Pi(t,s;x)$ is invertible from Ω to itself, there exists some $x_0\in\Omega$ such that $\Pi(t^*,0;x_0) = x^*$. Then for any $i=1,2$, we have

$$\begin{aligned} &u_i(t^*,\Pi(t^*,0;x_0)) \\ &\quad = u_i(0,x_0)\, e^{\int_0^{t^*} h_i((u_1,u_2)(l,\Pi(l,0;x_0)))+\frac{d}{\chi}(P(l,\Pi(l,0;x_0))-(u_1+u_2)(l,\Pi(l,0;x_0)))\mathrm{d}l} > 0, \end{aligned} \tag{2.13}$$

which implies

$$u_i(0,x_0) > 0, \quad i=1,2.$$

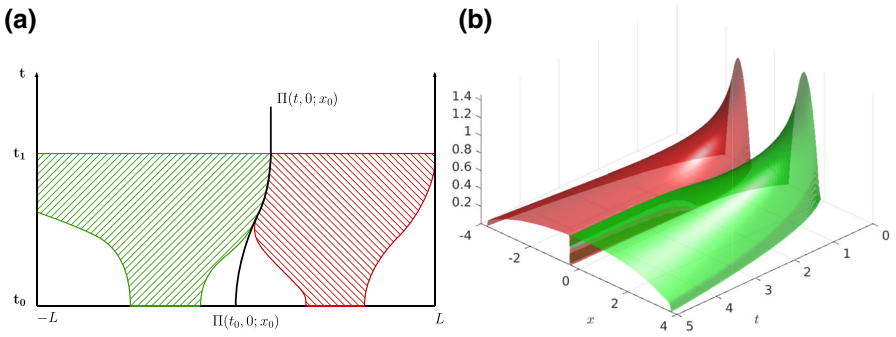

Fig. 5 In this figure we illustrate the notion of segregation with a one dimensional bounded domain. **a** The characteristic $t \mapsto \Pi(t, 0; x_0)$ forms a segregation "wall". **b** The temporal-spatial evolution of the two species

This is a contradiction. □

For the one dimensional case $N = 1$, suppose u_1, u_2 are solutions to (2.11)–(2.12), we give an illustration (see Fig. 5) of the segregation for the solutions integrated along the characteristics $u_i(t, \Pi(t, 0; x))$ for $i = 1, 2$. In fact, if there exists for some x_0 such that $u_i(0, x_0) = 0$ for $i = 1, 2$, then from Eq. (2.13) we obtain

$$u_1(t, \Pi(t, 0; x_0)) = u_2(t, \Pi(t, 0; x_0)) = 0, \ \forall t > 0.$$

Therefore, the characteristics $t \mapsto \Pi(t, 0; x_0)$ forms a segregation barrier for the two cell populations.

Remark 2.15 Our model can be regarded as an alternative to nonlinear diffusion models which also implements the finite speed propagation property. The local existence and uniqueness of solutions is proved rigorously in Appendix 5.2. The notion of solution integrated along the characteristics also leads to the segregation property.

Note that solutions starting from compactly supported initial value stay compactly supported for the single and multi-species models. This is a consequence of the notion of solution integrated along the characteristics together with the fact that the characteristics cannot blow up in finite time as long as the $W^{1,\infty}$ norm of the solution $u(t, \cdot)$ is finite for time t. Therefore, in our case, the finite speed propagation holds, which is similar to the models with nonlinear diffusion.

2.2.4 Conservation law on a volume

If we assume that $d_1 = d_2 = d$ in system (2.11), we have the following similar conservation law for two species case. Suppose volume $A \subset \Omega$ and each $0 \le s \le t$:

$$\int_{\Pi(t,s;A)} u_i(t, x)\mathrm{d}x = \int_A \exp\left[\int_s^t h_i\left((u_1, u_2)\left(l, \Pi(l, s; z)\right)\right)\mathrm{d}l\right] u_i(s, z)\mathrm{d}z, \quad i = 1, 2.$$

Therefore, if we assume in addition that $h_i = 0$ for any $0 \leq s \leq t$

$$\int_{\Pi(t,s;A)} u_i(t,x)\mathrm{d}x = \int_A u_i(s,z)\mathrm{d}z, \quad i = 1,2.$$

This means the total number of cells for each species u_i remains constant along the volume $\Pi(t,s;A)$.

3 Numerical simulations

In Sect. 2, we established a PDE model for two species and we also proved that the solution satisfies some basic properties such as local existence and uniqueness, positivity, segregation and conservation law. These properties are ideal to explain the monolayer cell co-culture in the experiments. Based on the data from experiments in Pasquier et al. (2011), we will fit some parameters in our model. By varying certain parameters such as the extra mortality rate caused by drug treatment (see Pasquier et al. 2011 for details), we will simulate the evolution of two populations in the Petri dish and the variation of population number of cells.

3.1 Impact of the segregation on the competitive exclusion principle

In this section, the goal of our simulations is to compare the various cases discussed in Proposition 2.12 (ODE case) with our PDE model with segregation. As we will see in the numerical simulations, the model with spatial structure presents completely different results compared to the ODE model. To that aim, we consider the case where the drug (doxorubicine) concentration is low in the cell co-culture for MCF-7 and MCF-7/Doxo (see Fig. 1). The drug treatment causes an additional mortality to the sensitive population MCF-7 represented by u_1 but no extra mortality to the resistant population MCF-7/Doxo represented by u_2 (MCF-7/Doxo is resistant to a small quantity of drug treatment, see Table 4 in Appendix 5.3).

We let U_i be the total number of cells in the u_i-population at time $t = 0$,

$$U_i = \int_\Omega u_i(0,x)\mathrm{d}x, \quad i = 1,2. \tag{3.1}$$

The parameter values used in the simulations and their interpretations are listed in Table 1. The growth rate b_i and the intraspecific competition a_{ii} are fitted to the data (see Appendix 5.3 for details).

In the presence of the drug, the equilibrium (2.10) of the ODE should be rewritten as

$$\bar{P}_1 = \frac{b_1 - \delta_1}{a_{11}}, \quad \bar{P}_2 = \frac{b_2 - \delta_2}{a_{22}}. \tag{3.2}$$

Table 1 List of parameters, their interpretations, values and symbols

Symbol	Interpretation	Value	Unit	Method	Dimensionless value
t	Time	1	day	–	1
r	Inner radius of the Petri dish	2.62	cm	Pasquier et al. (2011)	1
U_i	Total number of cells at $t = 0$	10^5	–	Pasquier et al. (2011)	0.01
b_1	Growth rate of cell u_1	0.6420	day^{-1}	Fitted	0.6420
b_2	Growth rate of cell u_2	0.6359	day^{-1}	Fitted	0.6359
a_{11}	Intraspecific competition of u_1	1.07×10^{-6}	cm^2/day	Fitted	1.5588
a_{22}	Intraspecific competition of u_2	1.06×10^{-6}	cm^2/day	Fitted	1.5415
d_1	Dispersion coefficient of u_1	13.73	cm^4/day	Fitted	2
d_2	Dispersion coefficient of u_2	13.73	cm^4/day	Fitted	2
χ	Sensing coefficient	6.86×10^{-2}	cm^2	Fitted	0.01

Here u_1 represents MCF-7 (sensitive cell) and u_2 represents MCF-7/Doxo (resistant cell). From Pasquier et al. (2011), the surface of the Petri dish is $21.5\,\text{cm}^2$. Thus the inner radius of the Petri dish r is calculated by $r^2\pi = 21.5\,\text{cm}^2$

Moreover, we assume the drug concentration is low, so that $b_1 - \delta_1 > 0$ and $\delta_2 = 0$, therefore we have

$$\bar{P}_1 < \bar{P}_2.$$

The case when $\bar{P}_1 > \bar{P}_2$ is similar and will be discussed in the end of this section. We choose our parameters to satisfy

$$\frac{a_{12}}{a_{11}} < \frac{\bar{P}_1}{\bar{P}_2}, \quad \frac{a_{21}}{a_{22}} < \frac{\bar{P}_2}{\bar{P}_1}, \tag{3.3}$$

which corresponds to Case (i) in Proposition 2.12 for the ODE system. By using (3.2), the condition in (3.3) can be interpreted as

$$\frac{a_{12}}{a_{22}} < \frac{b_1 - \delta_1}{b_2 - \delta_2}, \quad \frac{a_{21}}{a_{11}} < \frac{b_2 - \delta_2}{b_1 - \delta_1}.$$

Since we have $b_1 - \delta_1 > 0$ and $\delta_2 = 0$, if the coefficients a_{12} and a_{21} are small, then (3.3) holds. We give a possible set of parameters satisfying (3.3):

$$\delta_1 = 0.4, \quad \delta_2 = 0, \quad a_{12} = 0.2, \quad a_{21} = 1. \tag{3.4}$$

We assume the initial condition of each species u_i is composed of 20 circular cell clusters (represented by the red/green dots in Fig. 6a), uniformly distributed over the Petri dish Ω. The total number of cells is initially $U_i = 0.01$ (recall (3.1)) for each species and we assume that each cluster contains the same quantity of cells. We present the numerical simulation in Fig. 6 from day 0 to day 6. We also plot the proportions of cells in Fig. 6f, which are defined as

$$\frac{U_i(t)}{U_1(t) + U_2(t)}, \quad \text{where } U_i(t) := \int_\Omega u_i(t, x)\mathrm{d}x, \quad i = 1, 2,$$

for species i.

If the parameters are set as in (3.4) for the ODE system, Proposition 2.12 indicates that the two species are in the stable coexistence regime and the solution converges to the equilibrium

$$\bar{E}^* := \left(\frac{a_{22}(b_1 - \delta_1) - a_{12}(b_2 - \delta_2)}{a_{11}a_{22} - a_{12}a_{21}}, \frac{a_{21}(b_1 - \delta_1) - a_{11}(b_2 - \delta_2)}{a_{12}a_{21} - a_{11}a_{22}} \right) \approx (0.11, 0.34).$$

However, as shown in Fig. 6, we can see the population density u_1 tends to 0 and u_2 tends to 1. In particular, we observe the competitive exclusion principle for the PDE even though the solutions to the ODE are in the stable coexistence regime.

One can notice that unlike the ODE system (2.8), the segregation property for the PDE model implies that it is impossible for the two species to coexist at the same position $x \in \Omega$. Thus the coefficients a_{12}, a_{21} do not play any role in the competition

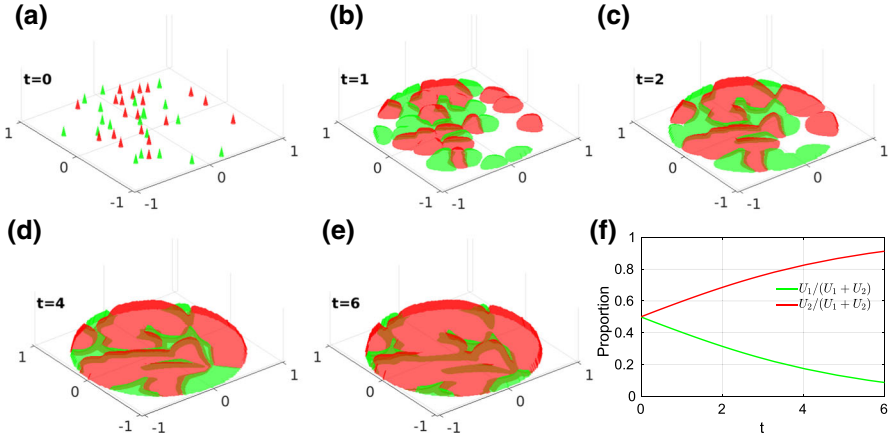

Fig. 6 Spatial-temporal evolution of the two species u_1 and u_2 and their proportions. **a**–**e** correspond to the evolution of cell growth form day 0 to day 6 and **f** is the plot of the proportion of each species in the total population from day 0 to day 6. We fix the parameters $\delta_1 = 0.4,\ \delta_2 = 0,\ a_{12} = 0.2,\ a_{21} = 1$ in (3.4). The initial condition is composed of 20 cell clusters which are uniformly distributed over the Petri dish. The initial total number of cells is $U_1 = U_2 = 0.01$ for each species and cells are equally distributed in each cluster. Other parameter values are listed in Table 1

because of the segregation principle. This is verified by numerical simulations: when we vary the coefficient coefficients a_{12}, a_{21}, we obtain identical plots for cell evolution and cell population ratio. Since the simulations are identical, we omitted them here.

Through the numerical simulations, we observed that the PDE model (2.11) undergoes a competitive exclusion principle. Our numerical simulations strongly indicate that the stable steady states only depend on the relation between $\bar{P}_1$ and $\bar{P}_2$ [see (3.2) for definition]. If $\bar{P}_1 < \bar{P}_2$ (resp. $\bar{P}_1 > \bar{P}_2$), the population u_2 (resp. u_1) will dominate and the other species will die out. We also simulated the case when $\bar{P}_1 > \bar{P}_2$, the results showed that $\bar{E}_1$ is the only stable steady state, which verifies our conjecture. As Proposition 2.12 shows, the stability of the equilibrium of the ODE system depends on the coefficients a_{12}, a_{21} which measure the interspecies competition. However, the stability of the steady states of the PDE system only depends on $\bar{P}_1$ and $\bar{P}_2$, which do not depend on a_{12}, a_{21}. This is a major difference between the ODE and PDE models.

3.2 Impact of the initial distribution on the final proportion of each species

In the previous section, we investigated the competitive exclusion principle for two species. By investigating Fig. 6f, we can see that the speed of increase in proportion of the dominant population u_2 (red curve) is varying with time. We remark that the increase of the dominant population u_2 is faster from day 0 to day 2 than from day 4 to day 6. If we further study the spatial-temporal evolution of the cell co-culture presented in Fig. 6a–e, we can observe that from day 0 to day 2 the competition between the two groups is mainly expressed in terms of competition for spatial resources. However, from day 4 to day 6, when the surface of the Petri dish is almost fully occupied by cells of either type, the reaction term $u_i h_i(u_1, u_2)$ in the equation begins to play a

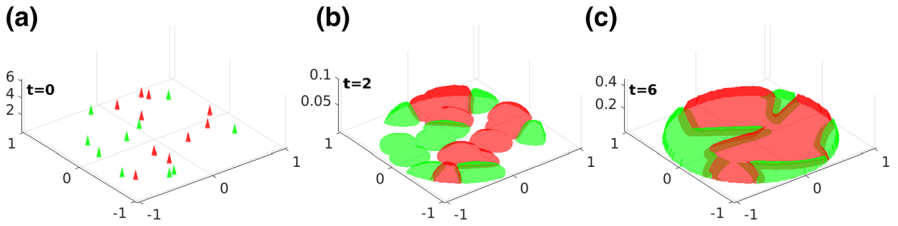

Fig. 7 Cell co-culture for species u_1 and u_2 over 6 days in the sparsely seeded case, i.e., $U_1 = U_2 = 0.005$, $N_{u_1} = N_{u_2} = 10$, for day 0, 2 and 6. Parameter values are listed in (3.5) and Table 1

major role in the change of the number of cells. In order to explore the major factors in cell competition, we investigate the impact on the initial distribution of cells on the proportion of each species on day 6. We will mainly focus on two factors, namely the initial number of cell clusters and the law of initial distribution of those clusters in space, which might influence the proportions for u_1 and u_2. To that aim, we set the following parameters

$$\delta_1 = 0.15, \quad \delta_2 = 0, \quad a_{12} = 0, \quad a_{21} = 0, \tag{3.5}$$

and fix the other parameters as in Table 1.

3.2.1 Dependency on the initial number of cell clusters

In cell culture, the initial number of cell clusters is an important factor. Bailey et al. (2018) study the sphere-forming efficiency of MCF-7 human breast cancer cell by comparing the cell culture with different initial numbers of cell clusters. Here we consider the impact of the initial number of cell clusters on the final proportion of each species. To that aim, we assume that the initial distribution follows the uniform distribution on a disk.

We consider two sets of initial condition, that is

$$U_1 = U_2 = 0.005, \quad N_{u_1} = N_{u_2} = 10, \tag{3.6}$$

$$U_1 = U_2 = 0.1, \quad N_{u_1} = N_{u_2} = 200, \tag{3.7}$$

where U_1 and U_2 are defined in (3.1) and N_{u_1} (respectively N_{u_2}) is the initial number of cell clusters of species u_1 (respectively, of species u_2).

The above initial conditions correspond to different types of seeding in the experiment, namely cells are sparsely seeded or densely seeded. We assume that the total number of cells is proportional to the initial number of cell clusters, meaning the dilution procedure adopted in the experiment is the same, thus the number of cells in each cell cluster is a constant. In Fig. 7, we first give a numerical simulation for the cell growth with parameters in (3.6). In Fig. 8, we present the simulation with parameters in (3.7), tracking from day 0 to day 6.

In Fig. 9 we plot the evolution of the total number of cells and the proportion of each species over 6 days.

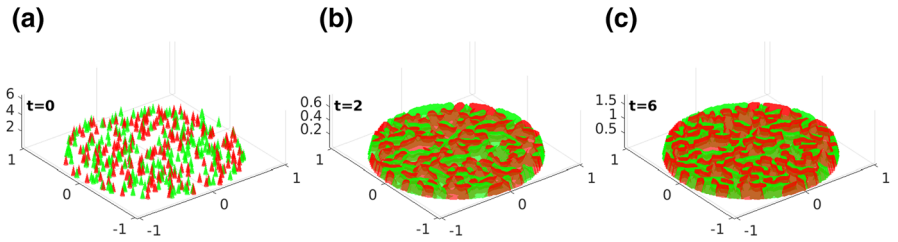

Fig. 8 Cell co-culture for species u_1 and u_2 over 6 days in the densely seeded case, i.e., $U_1 = U_2 = 0.1$, $N_{u_1} = N_{u_2} = 200$, for day 0, 2 and 6. Parameter values are listed in (3.5) and Table 1

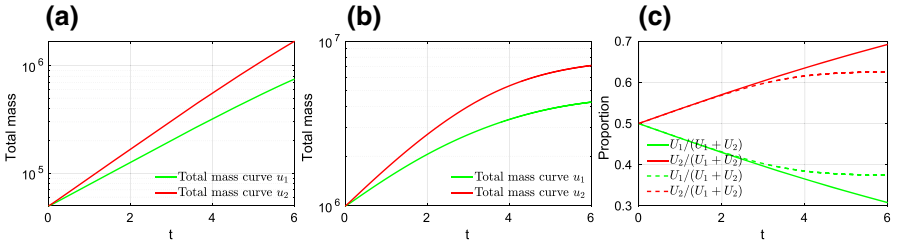

Fig. 9 Evolution of the total number of cells (in log scale) and their proportion for species u_1 and u_2 over 6 days. **a** corresponds to the sparsely seeded case [with parameter values as in (3.6)], **b** to the densely seeded case [with parameter values as in (3.7)]. In **c**, the solid lines represent the proportions of each species when we start with $N_{u_1} = N_{u_2} = 10$ and the dashed lines represent the proportions of each species when we start with $N_{u_1} = N_{u_2} = 200$. Parameters are listed in Table 1 and in (3.5)

From Fig. 9a, b, we can also observe a difference in the growth of each cell population. In Fig. 9a we can see that both cell populations are in the regime of exponential growth from day 0 to day 6 (a base-10 log scale is used for the y-axis). Conversely, in Fig. 9b the growth of each population is slowing down from day 4 to day 6, meaning that the cell co-culture is reaching the carrying capacity. More importantly, in Fig. 9c, we observe a significant difference in the development of proportion of each species. In fact, since the spatial competition is still the dominant factor in the first 2 days, we can hardly see any difference between the dashed lines and solid lines. The proportion of the dominant population grows almost linearly. However, the variation of the proportion of each species in the densely seeded case changes much slower after day 4, while the sparsely seeded group still varies linearly.

In the above numerical simulations, we considered the case where the total number of cells is proportional to the number of cell clusters. In the following numerical experiments, we fix the total number of cells, and vary only the number of cell clusters. By doing so, we intend to show the influence uniquely due to the number of cell clusters.

We consider two sets of initial condition, that is

$$U_1 = U_2 = 0.075, \quad N_{u_1} = N_{u_2} = 10, \tag{3.8}$$

$$U_1 = U_2 = 0.075, \quad N_{u_1} = N_{u_2} = 100, \tag{3.9}$$

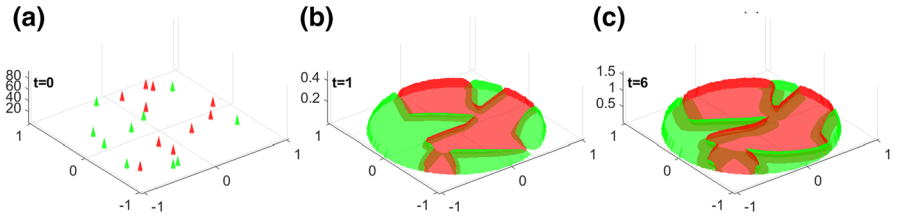

Fig. 10 Cell co-culture for species u_1 and u_2 over 6 days in the sparsely seeded case, i.e., $U_1 = U_2 = 0.075$, $N_{u_1} = N_{u_2} = 10$, for day 0, 1 and 6. Parameter values are listed in (3.5) and Table 1

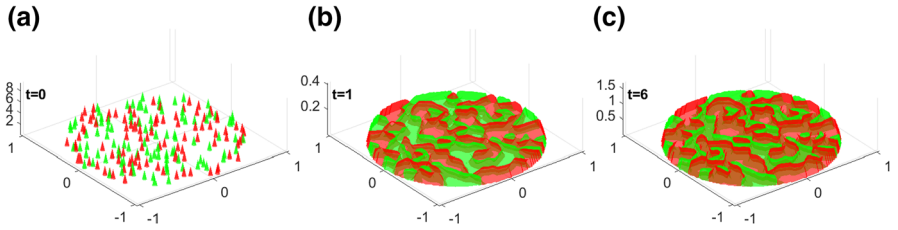

Fig. 11 Cell co-culture for species u_1 and u_2 over 6 days in the densely seeded case, i.e., $U_1 = U_2 = 0.075$, $N_{u_1} = N_{u_2} = 100$, for day 0, 1 and 6. Parameter values are listed in (3.5) and Table 1

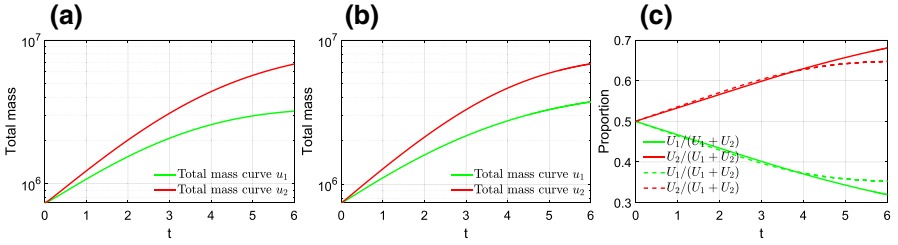

Fig. 12 Evolution of the total number (in log scale) and the proportion of each species u_1 and u_2 over 6 days. In **a** we plot the total number of each cell population corresponding to the simulations with parameters in (3.8) while **b** corresponds to the simulations with parameters in (3.9). In **c**, the solid lines represent the proportion of each species in the sparsely seeded case $N_{u_1} = N_{u_2} = 10$ and the dashed lines represent the proportion in the densely seeded case $N_{u_1} = N_{u_2} = 100$. Parameters are listed in Table 1 and (3.5)

where U_1 and U_2 are defined in (3.1) and N_{u_1} (respectively N_{u_2}) is the initial number of cell clusters of species u_1 (respectively species u_2).

The above initial conditions correspond to different types of seeding in the experiment, namely cells are sparsely seeded or densely seeded. We assume that the total number of cells is not proportional to the initial number of cell clusters, meaning that the dilution procedures adopted in the experiment are different, thus the number of cells in each cell cluster can be different.

In Fig. 10, we first give a numerical simulation for the cell growth with parameters in (3.8). In Fig. 11, we present the simulation with parameters in (3.9).

In Fig. 12 we plot the evolution of the total number of cells and the proportion of each species u_1 and u_2 over 6 days of the simulation.

The curves of the growth of the two cell populations in Fig. 12a, b are very similar. Both of them are reaching the carrying capacity (a base-10 log scale is used for the y-axis). However, as Fig. 12c shows, there is still a clear difference in the proportion of each species in the total population (dashed lines and solid lines) and this difference persists when we change the random seed for the uniform distribution at $t = 0$. In fact, as the total number of cells for the two scenarios is the same, the transition from the first expansion phase (from day 0 to day 1 in Figs. 10 and 11) to the second phase of the interspecies competition is very short for both two scenarios. During the first 4 days, we can hardly see any difference between the dashed lines and solid lines in Fig. 12c. The proportion of the dominant population grows almost linearly. However, the proportion of the densely seeded group slows down after day 4, while the sparsely seeded group still grows almost linearly. This difference can be more significant if we increase the difference of the initial number of clusters [see Fu (2019, page 119, Figures 3.7 and 3.8)].

Figures 10 and 11 show that when we start with the sparsely seeded condition, the species quickly expand to some large and connected clusters. On the contrary, for the densely seeded case, cells form small and scattered islets. Thus, even though the curves for the two scenarios are similar in Fig. 12a, b, the interactions of large clusters and small islets are different. This discrepancy can affect the competition between the two populations and eventually be expressed in the population ratio. As for the densely seeded case, though the competitive exclusion principle holds in this case, the time for the extinction of u_1 can be very long.

3.2.2 Dependency on the law of the initial distribution

In the experiment, the size of the Petri dish can be a factor to determine the law of the initial distribution for the cell. In general, under the same total number of cells, a small size Petri dish will lead to a biased initial distribution and cells are more likely to aggregate at the border. While a big Petri dish will make the cell distribution more homogeneous, closer to a uniform distribution. Therefore, in this section, we study whether the proportion of each species can be affected by the law of initial distribution.

We will assume that the center of each cluster in the initial distribution is given by its polar coordinates (r, θ), that the radius r follows the Beta distribution with parameters α and β, and that the angle θ is uniformly distributed in $[0, 2\pi]$. More precisely,

$$\{r_n\}_{n=1,\dots,N} \sim \text{Beta}(\alpha, \beta), \quad \{\theta_n\}_{n=1,\dots,N} \sim \text{U}(0, 2\pi).$$

Hence the Cartesian coordinates of the center of each cluster are given by

$$\begin{cases} x_n = \sqrt{r_n}\cos(\theta_n) \\ y_n = \sqrt{r_n}\sin(\theta_n) \end{cases} \qquad n = 1, 2, \dots, N. \tag{3.10}$$

In Fig. 13, we plot the density function of the Beta distribution for different α, β

$$f_{\alpha,\beta}(r) = 1/B(\alpha, \beta)\, r^{\alpha-1}(1-r)^{\beta-1},$$

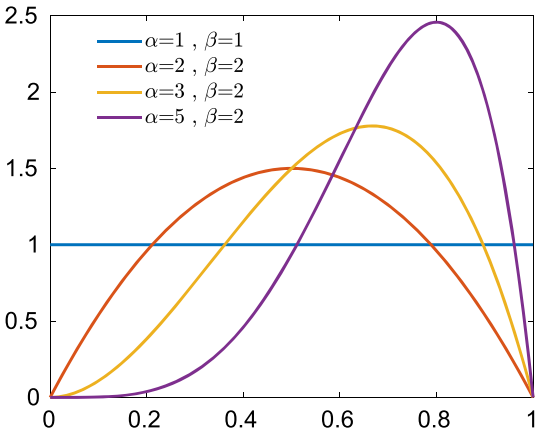

Fig. 13 Density function of the initial distribution $f_{\alpha,\beta}(r) = 1/B(\alpha, \beta)\, r^{\alpha-1}(1-r)^{\beta-1}$ for different α and β, where $B(\alpha, \beta)$ is a normalization constant to ensure that the total integral is 1

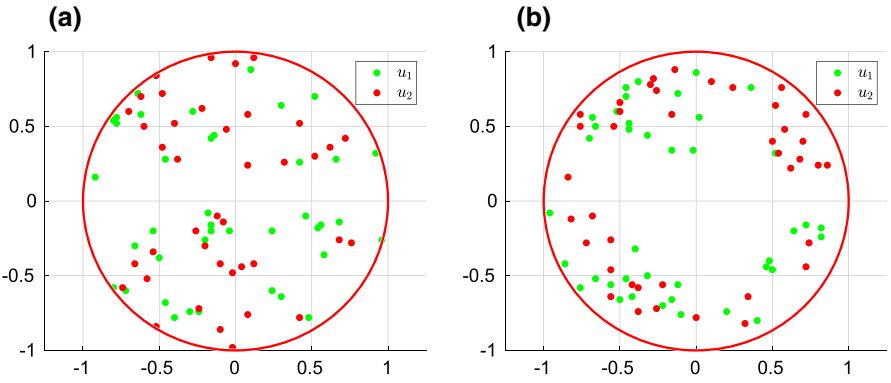

Fig. 14 Spatial distribution of the initial condition when $(\alpha, \beta) = (1, 1)$ (**a**) and $(\alpha, \beta) = (3, 2)$ (**b**). Here red dots and green dots represent cell clusters. The initial condition is composed of $N_{u_1} = 40$ and $N_{u_2} = 40$ cell clusters, in both cases (color figure online)

where $B(\alpha, \beta)$ is a normalization constant to ensure that the total mass is 1.

Our simulation will mainly compare the following two cases

$$(\alpha_1, \beta_1) = (1, 1), \quad (\alpha_2, \beta_2) = (3, 2).$$

We plot the initial distributions of the two different cases in Fig. 14 where we choose 40 cell clusters (i.e., $N_{u_1} = 40$ and $N_{u_2} = 40$ in (3.10)) for species u_1 and species u_2.

Suppose that the total number of cells $U_1 = U_2 = 0.02$ is equally distributed in each cell cluster. A typical numerical solution is shown in Fig. 15 when $(\alpha_1, \beta_1) = (1, 1)$ and in Fig. 16 when $(\alpha_2, \beta_2) = (3, 2)$.

Now we plot the evolution of the total number of cells for each species u_1 and u_2 over 6 days.

From Fig. 17 we can see that the law of initial distribution has almost no influence on the final proportion of species. We also tried different scenarios when the total number of cell clusters are 20, 50 and 100 or with different extra mortality rate $\delta_1 = 0, 0.2$ and

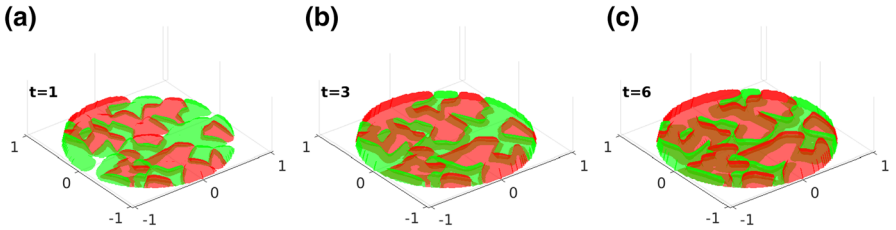

Fig. 15 Cell co-culture for species u_1 and u_2 over 6 days. We plot the case where the initial distribution follows beta distribution with parameters $(\alpha, \beta) = (1, 1)$. Parameters are listed in Table 1 and (3.5)

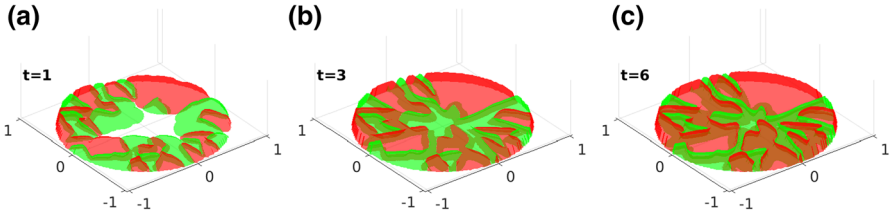

Fig. 16 Cell co-culture for species u_1 and u_2 over 6 days. We plot the case where the initial distribution follows beta distribution with parameters $(\alpha, \beta) = (3, 2)$. Parameters are listed in Table 1 and (3.5)

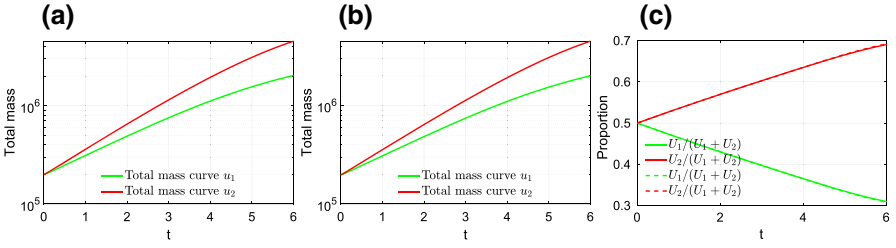

Fig. 17 Evolution of the total number of cells (in log scale) for species u_1 and u_2 and their proportions over 6 days. In **a** we plot the total number of cells corresponding to the uniform initial distribution in Fig. 15. In **b** we plot the number of cells corresponding to the initial distribution as in Fig. 16. In **c**, the solid lines represent the proportion when $(\alpha, \beta) = (1, 1)$ and the dashed lines represent the proportion in the case $(\alpha, \beta) = (3, 2)$. From **c**, we can see that they overlap. Parameters are listed in Table 1 and (3.5)

0.5, and the results are similar. Thus we can deduce that the final relative proportion is stable under the variation of the law of the initial distribution.

Combining the above numerical experiments in Sects. 3.2.1 and 3.2.2, we can see that under the competitive exclusion principle, the difference in the initial number of cell clusters can have an influence on the interspecific competition. To be more precise, with the same initial number of cells, the interspecific competition of the densely seeded group is different from the one in the sparsely seeded group.

3.3 Impact of the dispersion coefficient on the population ratio

In Sect. 3.2, when the parameters of the model are the same, the competition induced by the cell dynamics can be reflected by the difference in the spatial resource. Now we

Table 2 Two sets of dispersion coefficients for u_1 and u_2

Parameters	d_1	d_2	δ_1	δ_2
Scenario 1	2	2	0	0
Scenario 2	2	0.2	0	0

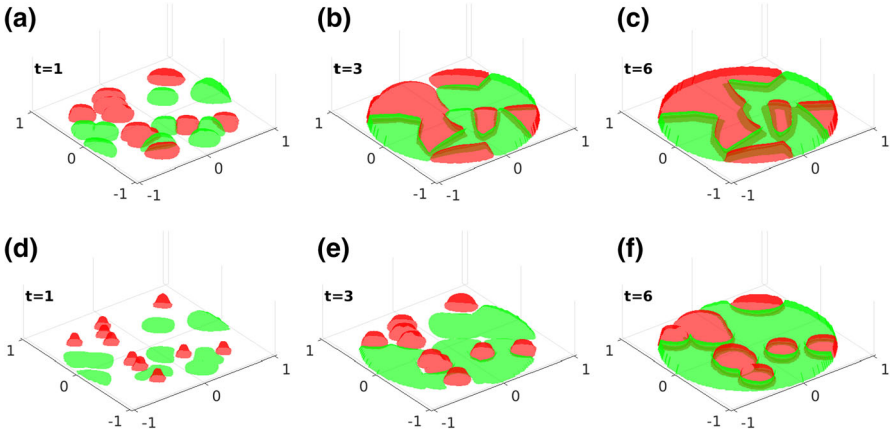

Fig. 18 Cell co-culture for species u_1 and u_2 over 6 days. **a**–**c** correspond to scenario 1 (i.e. with the parameters $d_1 = 2, d_2 = 2, \delta_1 = \delta_2 = 0$) while **d**–f correspond to scenario 2 (i.e. with $d_1 = 2, d_2 = 0.2, \delta_1 = \delta_2 = 0$). In both scenarios, the initial number of cell clusters and the total number of cells are the same and follow (3.11) and the same uniform distribution. We plot the simulations for day 1, 3 and day 6. Other parameters are listed in Table 1

assume the spatial resource is the same and we investigate the role of the dispersion coefficient in the evolution of the species.

To that aim, we let the initial distribution of the two species follow the same uniform distribution and they are sparsely seeded on the Petri dish. Furthermore, we let the cell dynamics for the two population be almost the same, the only variable we control here is the dispersion coefficient for the population. We take the same uniform initial distribution at day 0, with the same initial number of cell clusters and the same number of cells, i.e.,

$$U_1 = U_2 = 0.005, \quad N_{u_1} = N_{u_2} = 10, \quad a_{12} = a_{21} = 0. \tag{3.11}$$

We compare the following two scenarios in Table 2 where the only difference is the dispersion parameters.

In scenario 1, the dispersion coefficients of the two species are the same, while in scenario 2 we suppose the species u_1 has an advantage in the spatial competition over its competitor u_2 (Fig. 18).

Now we plot the evolution of the total number of cells and the proportion of each species for species u_1 and u_2 over 6 days.

The main result from Fig. 19 is that the dispersion coefficient can have a great impact on the proportion of each species after 6 days. Next, we consider the following

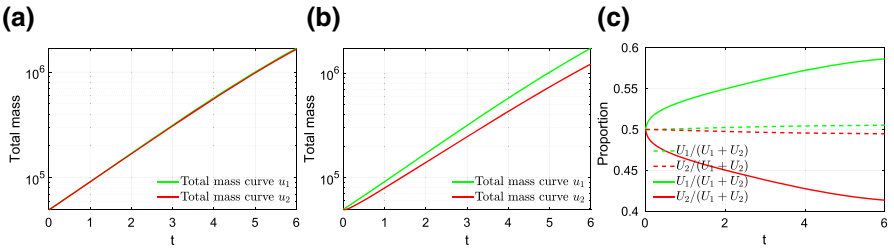

Fig. 19 Evolution of the total number of cells (in log scale) and the proportion in the total population for species u_1 and u_2 over 6 days. In **a** we plot the total number of cells corresponding to the scenario 1. In **b** we plot the total number of cells corresponding to the scenario 2. In **c** we plot the proportion of each species and the dashed lines corresponds to scenario 1 while the solid lines corresponds to scenario 2 in 2. Other parameters are listed in Table 1 and (3.11)

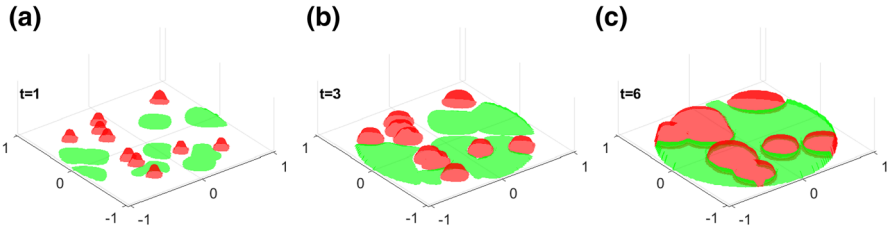

Fig. 20 Cell co-culture for species u_1 and u_2 over 6 days. **a**–**c** corresponds to the scenario 3 with $d_1 = 2, d_2 = 0.2, \delta_1 = 0.1, \delta_2 = 0$ in Table 3. The initial number of cell clusters and the total number of cells follow (3.11). Other parameters are listed in Table 1

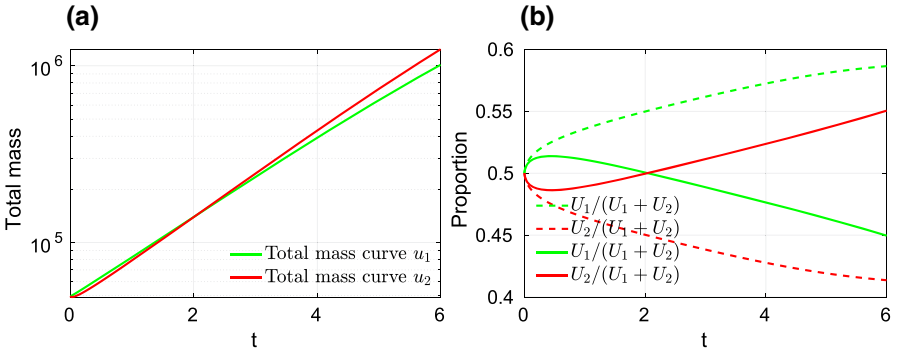

Fig. 21 Evolution of the total number of cells (in log scale) and the proportion of each species for species u_1 and u_2 over 6 days. In **a** we plot the total number of cells in scenario 3 (see Fig. 20). In **b**, the dashed lines correspond to the proportion of each species in the total population in scenario 2 with $d_1 = 2, d_2 = 0.2, \delta_1 = 0, \delta_2 = 0$ in Table 2 while the solid lines correspond to scenario 3 with $d_1 = 2, d_2 = 0.2, \delta_1 = 0.1, \delta_2 = 0$ in Table 3. Other parameters are listed in Table 1 and (3.11)

scenario where u_1 has the advantage in dispersion coefficient but is at a disadvantage induced by drug treatment. Therefore

By including now a drug treatment, we can see from Figs. 20 and 21 that between day 0 and day 2, the population u_1 dominates u_2 thanks to a larger dispersion rate. After day 2, since the drug is killing the cell for species u_1 while the drug has no effect

Table 3 This scenario corresponds to the case where the species u_1 spreads faster than the species u_2

Parameters	d_1	d_2	δ_1	δ_2
Scenario 3	2	0.2	**0.1**	0

Moreover, due to a drug treatment, the mortality of the species u_1 is strictly positive while the mortality of the species u_2 is zero (i.e. the drug treatment does not affect the second species). In the context of cancer cell, the species u_1 would correspond to cells which are sensitive to the drug while u_2 would correspond to the cell resistant to the drug treatment

on the species u_2, the species u_2 finally takes over the species u_1. It leads to a gradual increase in the proportion of the species u_2.

In the numerical simulations for the scenarios 1 and 2 in Table 2, we let the cell dynamics of the two species be almost equal. Thus the competition due to the cell dynamics is almost negligible. We have shown the dispersion coefficient of populations can have a great impact on the population ratio after 6 days.

In the simulation for scenario 3 in Table 3, we can observe that despite the competitive exclusion principle, a larger dispersion coefficient can lead to a short-term advantage in the population. In the long term, the competitive exclusion principle still dominates.

4 Conclusion and discussion

From the experimental data in the work of Pasquier et al. (2011), we modeled the mono-layer cell co-culture by a hyperbolic Keller–Segel equation (2.11). We proved the local existence and uniqueness of solutions by using the notion of the solution integrated along the characteristics in Theorem 2.7 and proved the conservation law in Theorem 2.9. For the asymptotic behavior, we analyzed the problem numerically in Sect. 3.

In Sect. 3.1 we discussed the competitive exclusion principle, indicating that the asymptotic behavior of the population depends only on the relationship between the steady states $\bar{P}_1$ and $\bar{P}_2$ [see (3.2) for definition] which is different from the ODE case. We found that except for the case $P_1 = P_2$, the model with spatial segregation always exhibits a competitive exclusion principle.

Even though the long term dynamics of cell density is decided by the relative values of the equilibrium, the short term behavior needs a more delicate description. We studied two factors which may influence the population ratios. The first factor is the initial cell distribution, as measured by the initial number of cell clusters and the law of initial distribution. We found that the impact of the initial distribution on the proportion of each species lies in the initial number of cell clusters but not in the law of initial distribution.

The second factor influencing the population ratio is the cell movement in space, as measured by the dispersion coefficient d_i. In the first stage (i.e. before the Petri dish is saturated), the dispersion rate d_i is the dominant factor. Once the surface of the Petri dish is saturated by cells, cell dynamics $u_i\, h(u_1, u_2)$ becomes the key factor.

Note that the coefficients a_{12}, a_{21} do not play any role in the competition because of the segregation principle.

We briefly summarize the main factors that can influence the population ratio in cell culture for model (2.11):

(a) The difference of cell dynamics in the two species (internal factor): if the equilibrium $\bar{P}_1 > \bar{P}_2$ (see (3.2) for definition), then u_1 will dominate, u_2 will die out (and vice-versa when $\bar{P}_1 < \bar{P}_2$) (see Fig. 6);
(b) If the initial number of cells is similar, the interspecific competition of the densely seeded group is different than the one of the sparsely seeded group (see Fig. 12). We also concluded that the law of initial distribution has almost no influence on the population ratio (see Figs. 15, 16);
(c) If cells are sparsely seeded at the beginning, the cell competition consists of two stages: the first stage, where the dispersion rate plays a major role, is for cells to occupy the surface of the Petri dish and the second stage, where the cell dynamics becomes the key factor, is for each species to reach a saturation stage (see Figs. 19, 21).

4.1 Mixed initial condition

In this paper, we are mainly focused on applying the model to the monolayer cell co-culture experiments in Pasquier et al. (2011) where the initial condition is always segregated. However, when the dispersion coefficients are the same $d_1 = d_2$ and the initial condition is mixed in the domain, the two population stay mixed even for large time, this can be proved by an argument similar to the one in Theorem 2.14. By Eq. (2.13),

$$u_i(t, \Pi(t,0;x)) = u_i(0,x) \exp\left(\int_0^t h_i((u_1,u_2)(l,\Pi(l,0;x))) + \frac{d}{\chi}(P(l,\Pi(l,0;x)) - (u_1+u_2)(l,\Pi(l,0;x)))\,\mathrm{d}l\right).$$

Therefore, if $u_1(0,x_0)u_2(0,x_0) > 0$, we can deduce $u_1(t,\Pi(t,0;x))u_2(t,\Pi(t,0;x)) > 0$ for any $t > 0$. To be more precise, if we take the time derivate of (2.13), we obtain

$$\frac{\mathrm{d}}{\mathrm{d}t}u_i(t,\Pi(t,0;x)) = u_i(t,\Pi(t,0;x))\Big(h_i((u_1,u_2)(t,\Pi(t,0;x))) + \frac{d}{\chi}\big(P(t,\Pi(t,0;x)) - (u_1+u_2)(t,\Pi(t,0;x))\big)\Big).$$

Note that both solutions $u_i(t,\Pi(t,0;x))$, $i = 1,2$ have a common term $\frac{d}{\chi}(P(t,\Pi(t,0;x)) - (u_1+u_2)(t,\Pi(t,0;x)))$. Therefore, for those mixed (non-segregated) initial condition, it is the term $h_i((u_1,u_2)(t,\Pi(t,0;x)))$ that determines the competition between these two species.

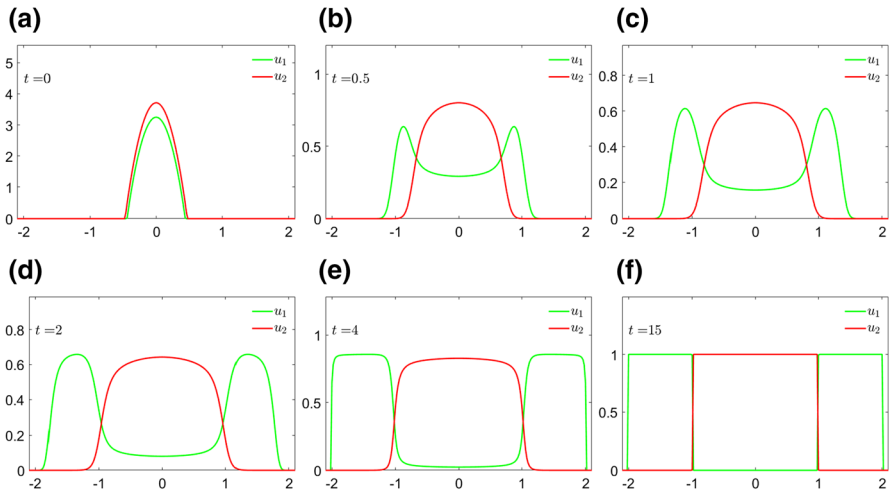

Fig. 22 Evolution of two species under a toy model (4.1) with mixed initial condition. The dispersion rate $d_1 = 2$ while $d_2 = 1$. For $t > 15$, the distributions $u_1(t, .)$ and $u_2(t, .)$ are almost independent of t. The numerical results suggest that asymptotic segregation occurs

When $d_1 \neq d_2$, it is interesting to show some further numerical simulations with mixed initial condition. Our numerical simulations suggest that segregation occurs asymptotically. We present numerical results of asymptotic segregation in Fig. 22, which were obtain by simulating the following toy model

$$\begin{cases} \partial_t u_1(t,x) - d_1 \operatorname{div}\big(u_1(t,x)\nabla P(t,x)\big) = u_1(t,x)\,(1 - u_1(t,x) - 2u_2(t,x)) \\ \partial_t u_2(t,x) - d_2 \operatorname{div}\big(u_2(t,x)\nabla P(t,x)\big) = u_2(t,x)\,(1 - 2u_1(t,x) - u_2(t,x)) \quad \text{in } [0,T]\times[-2,2] \\ \big(I-\Delta\big)P(t,x) = u_1(t,x) + u_2(t,x) \\ \nabla P(t,x)\cdot \nu(x) = 0 \qquad\qquad\qquad\qquad\qquad\qquad\qquad\qquad \text{on } [0,T]\times\{-2,2\}, \end{cases} \tag{4.1}$$

where we set $T = 15$ and $d_1 = 2$ and $d_2 = 1$.

Acknowledgements The authors would like to thank the referees for their valuable comments and suggestions.

5 Appendix

5.1 Invariance of domain Ω

In this section, we prove the invariance of domain Ω for the characteristic equation.

Assumption 5.1 *Let $\Omega \subset \mathbb{R}^2$ be an open bounded subset with $\partial\Omega$ of class C^2.*

Since Ω is a bounded domain of class C^2, there exists U a neighborhood of the boundary $\partial\Omega$ such that the distance function $x \to \operatorname{dist}(x, \partial\Omega) := \inf_{y\in\partial\Omega} \|x - y\|$ restricted to U has the regularity C^2 [see Foote (1984, Theorem 1)]. Furthermore,

by Foote (1984, Theorem 1) and Ambrosio (2000, Theorem 1 p.11), we have the following properties for Ω.

Lemma 5.2 *Let Assumption 5.1 be satisfied. Then*

(i) *There exists a small neighborhood U of $\partial\Omega$ with $U \subset \overline{\Omega}$ such that, for every $x \in U$ there is a unique projection $P(x) \in \partial\Omega$ satisfying* $\operatorname{dist}(x, P(x)) = \operatorname{dist}(x, \partial\Omega)$.
(ii) *The distance function $x \mapsto \delta(x) := \operatorname{dist}(x, \partial\Omega)$ is C^2 on $U \backslash \partial\Omega$.*
(iii) *For any $x \in U$, $\nabla\delta(x) = -\nu(P(x))$ where $\nu(x)$ is the outward normal vector.*

We consider the following non-autonomous differential equation on Ω

$$\begin{cases} x'(t) = f(t, x(t)) & t > 0 \\ x(0) = x_0 \in \Omega. \end{cases} \tag{5.1}$$

Assumption 5.3 *The vector field $f : [0, \infty) \times \overline{\Omega} \to \mathbb{R}^2$ is continuous and satisfies*

$$\nu(x) \cdot f(t, x) \leq 0, \quad \forall t > 0, \ \forall x \in \partial\Omega. \tag{5.2}$$

Moreover, for any $T > 0$, there exists a constant $K = K(T)$ such that vector field f satisfies

$$|f(t, x) - f(t, y)| \leq K|x - y|, \quad \forall x, y \in \overline{\Omega}, \ t \in [0, T]. \tag{5.3}$$

By (5.3), we have the existence and uniqueness of the solutions of (5.1) and the solutions may eventually reach the boundary $\partial\Omega$ in finite time. We will prove that (5.2) implies that the solutions of (5.1) actually stay in Ω and can not attain boundary $\partial\Omega$ in finite time under Assumption 5.1.

Theorem 5.4 *Let Assumptions 5.1 and 5.3 be satisfied. For any $T > 0$, let $x(t)$ be the solution of (5.1) on $[0, T]$. Then $x(t) \in \Omega$ for any $t \in [0, T]$.*

Proof We prove this theorem by contradiction. Let $t^* \in (0, T]$ be the first time when $x(t)$ reaches boundary $\partial\Omega$, i.e.,

$$t^* = \inf\{0 < t \leq T : \delta(x(t)) = 0\}.$$

We can find a $\theta > 0$ such that, $x(t) \in U \cap \overline{\Omega}$ for any $t \in [t^* - \theta, t^*]$. Since $t \to x(t)$ is C^1, the mapping $t \mapsto \delta(x(t))$ is C^1 on $[t^* - \theta, t^*]$. By Lemma 5.2(iii), we have

$$\frac{d}{dt}\delta(x(t)) = x'(t) \cdot \nabla\delta(x(t)) = -f(t, x(t)) \cdot \nu(y(t)), \tag{5.4}$$

where ν is the outward normal vector and $y(t) := P_{\partial\Omega}(x(t))$ is the unique projection of $x(t)$ onto $\partial\Omega$. By assumption (5.2), we have

$$\begin{aligned} -f(t, x(t)) \cdot \nu(y(t)) &= \big(f(t, y(t)) - f(t, x(t))\big) \cdot \nu(y(t)) - f(t, y(t)) \cdot \nu(y(t)) \\ &\geq \big(f(t, y(t)) - f(t, x(t))\big) \cdot \nu(y(t)). \end{aligned}$$

Hence (5.4) becomes

$$\begin{aligned}\frac{d}{dt}\delta(x(t)) &= -f(t,x(t))\cdot v(y(t))\\ &\geq \big(f(t,y(t))-f(t,x(t))\big)\cdot v(y(t))\\ &\geq -|f(t,y(t))-f(t,x(t))|\,|v(y(t))|\\ &\geq -K|y(t)-x(t)| = -K\delta(x(t)),\quad t\in[t^*-\theta,t^*],\end{aligned}$$

which yields

$$\delta(x(t)) \geq \delta(x(t^*-\theta))e^{-K(t-t^*+\theta)},\quad \forall t\in[t^*-\theta,t^*],$$

and $\delta(x(t^*-\theta)) > 0$ implies $\delta(x(t^*)) > 0$ which contradicts our assumption $\delta(x(t^*)) = 0$. □

5.2 Proof of Theorem 2.7

The objective of Appendix 5.2 is to give a clear notion of solutions and to prove the local existence and uniqueness of solution.

Solution integrated along the characteristics Let us temporarily suppose $u \in C^1([0,T]\times\Omega)$, we can rewrite the first equation in (2.1) as

$$\begin{aligned}\partial_t u(t,x) - d\,\nabla u(t,x)\cdot\nabla P(t,x) &= u(t,x)h(u(t,x)) + d\,u(t,x)\Delta P(t,x)\\ &= u(t,x)\left(h(u(t,x)) + \frac{d}{\chi}(P(t,x)-u(t,x))\right).\end{aligned}$$

Moreover, if we differentiate the solution along the characteristic with respect to t then

$$\begin{aligned}&\frac{\mathrm{d}}{\mathrm{d}t}u(t,\Pi(t,0;x))\\ &\quad= \partial_t u(t,\Pi(t,0;x)) + \nabla u(t,\Pi(t,0;x))\cdot\partial_t\Pi(t,0;x)\\ &\quad= \partial_t u(t,\Pi(t,0;x)) - d\,\nabla u(t,\Pi(t,0;x))\cdot\nabla P(t,\Pi(t,0;x))\\ &\quad= u(t,\Pi(t,0;x))\left(h(u(t,\Pi(t,0;x))) + \frac{d}{\chi}\left(P(t,\Pi(t,0;x)) - u(t,\Pi(t,0;x))\right)\right).\end{aligned}$$

The solution along the characteristics can be written as

$$\begin{aligned}&u(t,\Pi(t,0;x))\\ &\quad= u_0(x)\exp\left(\int_0^t h(u(l,\Pi(l,0;x))) + \frac{d}{\chi}\big(P(l,\Pi(l,0;x)) - u(l,\Pi(l,0;x))\big)\mathrm{d}l\right).\end{aligned}$$

Similarly, we can deduce for any $0\leq s\leq t$

$$u(t, \Pi(t, s; x)) = u(s, x) \exp\left(\int_s^t h(u(l, \Pi(l, s; x))) + \frac{d}{\chi}\big(P(l, \Pi(l, s; x)) - u(l, \Pi(l, s; x))\big)\mathrm{d}l\right). \tag{5.5}$$

For the simplicity of notation, we let $d = \chi = 1$ in our following discussion and define $w(t, x) := u(t, \Pi(t, 0; x))$. We construct the following Banach fixed point problem for the pair (w, P). For each (w, P), we let

$$w^1(t, x) = u_0(x) \exp\left(\int_0^t F(w(l, x)) + P(l, \Pi(l, 0; x))\mathrm{d}l\right). \tag{5.6}$$

where we set $F(u) = h(u) - u$ for any $u \geq 0$ and we define

$$\mathcal{T}\begin{pmatrix} w(t, x) \\ P(t, x) \end{pmatrix} := \begin{pmatrix} w^1(t, x) \\ (I - \Delta)^{-1} w^1(t, \Pi(0, t; x)) \end{pmatrix} = \begin{pmatrix} w^1(t, x) \\ P^1(t, x) \end{pmatrix}, \tag{5.7}$$

where $(I - \Delta)^{-1}$ is the resolvent of the Laplacian operator with Neumann boundary condition.

We define

$$\begin{aligned} X^\tau &:= C^0\big([0, \tau], C^0(\overline{\Omega})\big), \quad Y^\tau := C^0\big([0, \tau], C^1(\overline{\Omega})\big), \\ \tilde{X}^\tau &:= \left\{ w \in C^0\big([0, \tau], C^0(\overline{\Omega})\big) \;\middle|\; w \geq 0, \sup_{t \in [0, \tau]} \|w(t, \cdot)\|_{W^{1,\infty}(\Omega)} \leq C_1 \right\}, \\ \tilde{Y}^\tau &:= \left\{ P \in C^0\big([0, \tau], C^1(\overline{\Omega})\big) \;\middle|\; \sup_{t \in [0, \tau]} \big\|P(t, \cdot)\big\|_{W^{2,\infty}(\Omega)} \leq C_2 \right\}, \end{aligned} \tag{5.8}$$

where $C_i, i = 1, 2$ are two constants to be fixed later. We also set

$$Z^\tau := X^\tau \times Y^\tau, \quad \tilde{Z}^\tau := \tilde{X}^\tau \times \tilde{Y}^\tau.$$

Notice $\tilde{Z}^\tau$ is a complete metric space for the distance induced by the norm $(\|\cdot\|_{X^\tau}, \|\cdot\|_{Y^\tau})$. For simplicity, we denote $\|\cdot\|_{C^{\alpha,k}} := \|\cdot\|_{C^{\alpha,k}(\Omega)}$ and $\|\cdot\|_{W^{k,\infty}} := \|\cdot\|_{W^{k,\infty}(\Omega)}$ for $\alpha \in (0, 1], k \in \mathbb{N}_+$.

Theorem 5.5 (Existence and uniqueness of solutions) *For any initial value $u_0 \in W^{1,\infty}(\Omega)$ and $u_0 \geq 0$, for any C_1, C_2 large enough in (5.8), there exists $\tau = \tau(C_1, C_2) > 0$ such that the mapping $\mathcal{T}$ has a unique fixed point in $\tilde{Z}^\tau$.*

Proof For any positive initial value $u_0 \in W^{1,\infty}(\Omega)$ and $r > 0$, we fix C_1 to be a constant such that $4\|u_0\|_{W^{1,\infty}} \leq C_1$ and C_2 is a constant defined in (5.19) later in the proof.

We also denote

$$\begin{pmatrix} w^0 \\ P^0 \end{pmatrix} = \begin{pmatrix} u_0 \\ (I - \Delta)_{\mathcal{N}}^{-1} u_0 \end{pmatrix}$$

and let $\overline{B_{\tilde{Z}^\tau}}\left(\begin{pmatrix} w^0 \\ P^0 \end{pmatrix}, r\right)$ be the closed ball centered at $\begin{pmatrix} w^0 \\ P^0 \end{pmatrix}$ with radius r in $\tilde{Z}^\tau = \tilde{X}^\tau \times \tilde{Y}^\tau$ with usual product norm

$$\left\| \begin{pmatrix} w \\ P \end{pmatrix} \right\|_{\tilde{Z}^\tau} := \|w\|_{X^\tau} + \|P\|_{Y^\tau}$$

and we set

$$\kappa := \left\| \begin{pmatrix} w^0 \\ P^0 \end{pmatrix} \right\|_{\tilde{Z}^\tau} + r.$$

Suppose $\begin{pmatrix} w \\ P \end{pmatrix} \in \overline{B_{Z^\tau}}\left(\begin{pmatrix} w^0 \\ P^0 \end{pmatrix}, r\right)$, we need to prove that there exits a τ small enough such that the following properties hold

(a) For any $t \in [0, \tau]$, $\left(w^1(t, \cdot), P^1(t, \cdot)\right)$ in (5.6) and (5.7) belong to $W^{1,\infty}(\Omega) \times W^{2,\infty}(\Omega)$ and their norms satisfy

$$\sup_{t\in[0,\tau]} \|w^1(t, \cdot)\|_{W^{1,\infty}} \le C_1, \tag{5.9}$$

$$\sup_{t\in[0,\tau]} \|P^1(t, \cdot)\|_{W^{2,\infty}} \le C_2. \tag{5.10}$$

(b) Moreover, we have

$$\|w^1 - w^0\|_{X^\tau} \le \frac{r}{2}, \tag{5.11}$$

$$\|P^1 - P^0\|_{Y^\tau} \le \frac{r}{2}. \tag{5.12}$$

Moreover, we plan to show that the mapping is a contraction: there exists a $\theta \in (0, 1)$ such that for any $\begin{pmatrix} \tilde{w} \\ \tilde{P} \end{pmatrix}, \begin{pmatrix} w \\ P \end{pmatrix} \in \overline{B_{\tilde{Z}^\tau}}\left(\begin{pmatrix} w^0 \\ P^0 \end{pmatrix}, r\right)$ we have

$$\left\| \mathcal{T}\begin{pmatrix} \tilde{w} \\ \tilde{P} \end{pmatrix} - \mathcal{T}\begin{pmatrix} w \\ P \end{pmatrix} \right\|_{\tilde{Z}^\tau} \le \theta \left\| \begin{pmatrix} \tilde{w} \\ \tilde{P} \end{pmatrix} - \begin{pmatrix} w \\ P \end{pmatrix} \right\|_{\tilde{Z}^\tau}. \tag{5.13}$$

Step 1 We show that there exists a τ small enough such that for any $(w, P) \in \tilde{X}^\tau \times \tilde{Y}^\tau$ then

$$\sup_{t\in[0,\tau]} \|w^1(t, \cdot)\|_{W^{1,\infty}} \le C_1,$$

where w^1 is defined in (5.6).

Indeed, since $\nabla P(t,\cdot)$ is Lipschitz continuous, then $x \to \Pi(t,0,x)$ is also Lipschitz continuous. Since $\Pi(t,0;\cdot)$ maps Ω into Ω, we have

$$\begin{aligned}\|P(t,\Pi(t,0;\cdot))\|_{W^{1,\infty}} &\le \|P(t,\Pi(t,0;\cdot))\|_{L^\infty} + \|\nabla P(t,\cdot)\|_{L^\infty}\|\Pi(t,0;\cdot)\|_{W^{1,\infty}}\\ &\le \|P(t,\cdot)\|_{W^{1,\infty}}\max\{\|\Pi(t,0;\cdot)\|_{W^{1,\infty}},1\}.\end{aligned}$$

For any $t\in[0,\tau]$, we let $\tilde{F} := \sup_{u\in[0,\kappa]}\{|F(u)|+|F'(u)|\}$. By the definition of w^1 in (5.6), we have

$$\begin{aligned}&\|w^1(t,\cdot)\|_{W^{1,\infty}}\\ &\le \|u_0\|_{W^{1,\infty}}\left\|\exp\left\{\int_0^t F(w(l,\cdot))+P(l,\Pi(l,0,\cdot))\mathrm{d}l\right\}\right\|_{W^{1,\infty}}\\ &\le \|u_0\|_{W^{1,\infty}}\left\|\exp\left\{\int_0^t F(w(l,\cdot))+P(l,\Pi(l,0,\cdot))\mathrm{d}l\right\}\right\|_{L^\infty}\\ &\quad\times\left(1+\int_0^t \|F(w(l,\cdot))\|_{W^{1,\infty}}+\|P(l,\Pi(l,0,\cdot))\|_{W^{1,\infty}}\mathrm{d}l\right)\\ &\le \|u_0\|_{W^{1,\infty}}\exp\left\{\int_0^t \|F(w(l,\cdot))\|_{L^\infty}+\|P(l,\Pi(l,0,\cdot))\|_{L^\infty}\mathrm{d}l\right\}\\ &\quad\times\left(1+\tau\tilde{F}\max\{\sup_{l\in[0,\tau]}\|w(l,\cdot)\|_{W^{1,\infty}},1\}+\tau\|P(l,\cdot)\|_{W^{1,\infty}}\max\{\|\Pi(l,0,\cdot)\|_{W^{1,\infty}},1\}\right)\\ &\le \|u_0\|_{W^{1,\infty}}e^{\tau\left(\tilde{F}+\kappa\right)}\left(1+\tau\tilde{F}\max\{C_1,1\}+\tau\kappa\max\{\|\Pi(l,0,\cdot)\|_{W^{1,\infty}},1\}\right).\end{aligned}\tag{5.14}$$

Next we estimate $\max\left\{\sup_{l\in[0,\tau]}\|\Pi(l,0,\cdot)\|_{W^{1,\infty}},1\right\}$. We have for any $t,s\in[0,\tau]$

$$\Pi(t,s;x) = x - \int_s^t \nabla P(l,\Pi(l,s;x))\mathrm{d}l.$$

Since Ω is the unit open disk, $\|x\|_{W^{1,\infty}(\Omega)} = 2$. We can obtain the following estimate

$$\begin{aligned}\|\Pi(t,s;\cdot)\|_{W^{1,\infty}} &\le 2+\int_s^t \|\nabla P(l,\Pi(l,s;\cdot))\|_{W^{1,\infty}}\mathrm{d}l\\ &\le 2+\sup_{l\in[s,t]}\|\nabla P(l,\cdot)\|_{W^{1,\infty}}\int_s^t \max\left\{\|\Pi(l,s;\cdot)\|_{W^{1,\infty}},1\right\}\mathrm{d}l\\ &\le 2+C_2\int_s^t \max\{\|\Pi(l,s;\cdot)\|_{W^{1,\infty}},1\}\mathrm{d}l.\end{aligned}$$

Thanks to Grönwall's inequality, we have

$$\sup_{t,s\in[0,\tau]}\|\Pi(t,s;\cdot)\|_{W^{1,\infty}} \le 2e^{\tau C_2}.\tag{5.15}$$

Substituting the (5.15) into (5.14) yields

$$\|w^1(t,\cdot)\|_{W^{1,\infty}} \le \|u_0\|_{W^{1,\infty}} e^{\tau\left(\tilde{F}+\kappa\right)}\left(1+\tau\tilde{F}\max\{C_1,1\}+2\tau\kappa e^{\tau C_2}\right).$$

Since $C_1 \ge 4\|u_0\|_{W^{1,\infty}}$, we can choose $\tau \le \min\left\{\frac{\ln 2}{\tilde{F}+\kappa}, \frac{1}{\tilde{F}\max\{C_1,1\}+2\kappa e^{C_2}}, 1\right\}$ and we obtain

$$\sup_{t\in[0,\tau]} \|w^1(t,\cdot)\|_{W^{1,\infty}} \le C_1. \tag{5.16}$$

Thus, Eq. (5.9) holds.

Let us now check that w^1 satisfies (5.11). Let $\chi[u] := ue^u$, we remark that $|e^u-1| \le ue^u = \chi[u]$ for all $u \ge 0$. We have

$$\begin{aligned}
|w^1(t,x)-u_0(x)| &\le |u_0(x)|\left|\exp\left\{\int_0^t F(w(l,x))+P(l,\Pi(l,0,x))\mathrm{d}l\right\}-1\right| \\
&\le \|u_0\|_{C^0}\chi\left[\int_0^t \|F(w(l,\cdot))\|_{C^0}+\|P(l,\Pi(l,0,\cdot))\|_{C^0}\mathrm{d}l\right] \\
&\le \|u_0\|_{C^0}\chi\left[\tau\tilde{F}+\tau\sup_{l\in[0,\tau]}\|P(l,\cdot)\|_{C^0}\right] \\
&\le \|u_0\|_{C^0}\chi\left[\tau\tilde{F}+\tau\kappa\right],
\end{aligned} \tag{5.17}$$

where $\tilde{F} = \sup_{u\in[0,\kappa]}\left\{|F(u)|+|F'(u)|\right\}$. From (5.17) we have

$$\sup_{t\in[0,\tau]} \|w^1(t,\cdot)-u_0(\cdot)\|_{C^0} \le \|u_0\|_{C^0}\chi\left[\tau\tilde{F}+\tau\kappa\right]. \tag{5.18}$$

Since $\lim_{u\to 0}\chi[u]=0$, it suffice to take τ small enough to ensure (5.11).

Step 2 Next we verify (5.10) and (5.12) for P^1 where P^1 is defined as the second component of (5.7). We show that there exists τ small enough such that for any $(w,P) \in \tilde{X}^\tau \times \tilde{Y}^\tau$

$$\sup_{t\in[0,\tau]} \|P^1(t,\cdot)\|_{W^{2,\infty}} \le C_2.$$

Thanks to the Schauder estimate (Gilbarg and Trudinger 2001, Theorem 6.30), there exists a constant C depending only on Ω such that

$$\|P^1(t,\cdot)\|_{C^{2,\frac{1}{2}}} \le C\|w^1(t,\Pi(0,t;\cdot))\|_{C^{0,\frac{1}{2}}}.$$

Recalling $\sup_{t\in[0,\tau]}\|\Pi(0,t;\cdot)\|_{W^{1,\infty}} \le 2e^{\tau C_2}$ as a consequence of (5.15), we have

$$\|P^1(t,\cdot)\|_{W^{2,\infty}} \le \|P^1(t,\cdot)\|_{C^{2,\frac{1}{2}}}$$

$$
\begin{aligned}
&\le C\|w^1(t,\Pi(0,t;\cdot))\|_{C^{0,\frac{1}{2}}}\\
&\le C\|w^1(t,\Pi(0,t;\cdot))\|_{W^{1,\infty}}\\
&\le C\|w^1(t,\cdot)\|_{W^{1,\infty}}\max\{\|\Pi(0,t;\cdot)\|_{W^{1,\infty}},1\}\\
&\le 2\,C\,C_1 e^{\tau C_2}.
\end{aligned}
$$

We can now define

$$C_2 = 4\,C\,C_1, \tag{5.19}$$

which only depends on Ω and $\|u_0\|_{W^{1,\infty}}$. Finally, we let $\tau \le (\ln 2)/C_2$ and we have

$$\|P^1(t,\cdot)\|_{W^{2,\infty}} \le 4\,C\,C_1 = C_2.$$

In particular, we have shown (5.10).

Next we prove (5.12). Since Ω is a two-dimensional unit disk, using Morrey's inequality (Evans 1998, Chapter 5. Theorem 6), we have

$$\|P^1(t,\cdot) - P_0(\cdot)\|_{C^{1,\frac{1}{2}}} \le C\|P^1(t,\cdot) - P_0(\cdot)\|_{W^{2,4}},$$

where C is a constant depending only on Ω. For the sake of simplicity, we use the same notation C for a universal constant depending only on Ω in the following estimates. Moreover, by the classical elliptic estimates we have

$$\|P^1(t,\cdot) - P_0(\cdot)\|_{W^{2,4}} \le C\|w^1(t,\Pi(0,t;\cdot)) - u_0(\cdot)\|_{L^4}.$$

This implies that

$$
\begin{aligned}
\|P^1(t,\cdot) - P_0(\cdot)\|_{C^1} &\le C\|w^1(t,\Pi(0,t;\cdot)) - u_0(\cdot)\|_{L^4}\\
&\le C\|w^1(t,\Pi(0,t;\cdot)) - u_0(\cdot)\|_{C^0}\\
&\le C\|w^1(t,\Pi(0,t;\cdot)) - w^1(t,\cdot)\|_{C^0} + C\|w^1(t,\cdot) - u_0(\cdot)\|_{C^0}\\
&\le C\|w^1\|_{W^{1,\infty}}\|\Pi(0,t;\cdot) - \cdot\|_{C^0} + C\|w^1(t,\cdot) - u_0(\cdot)\|_{C^0}\\
&\le C\;C_1\|\Pi(0,t;\cdot) - \cdot\|_{C^0} + C\|w^1(t,\cdot) - u_0(\cdot)\|_{C^0}\\
&\le C\;C_1\;\tau \sup_{t\in[0,\tau]}\|\nabla P(t,\cdot)\|_{C^0} + C\|w^1(t,\cdot) - u_0(\cdot)\|_{C^0}\\
&\le C\;C_1\;\tau\;\kappa + C\|w^1(t,\cdot) - u_0(\cdot)\|_{C^0}\\
&\le C\;C_1\;\tau\;\kappa + C\|u_0\|_{C^0}\chi\left[\tau\tilde{F} + \tau\kappa\right],
\end{aligned}
$$

where we have used (5.18) for the last inequality . We can conclude

$$\sup_{t\in[0,\tau]}\|P^1(t,\cdot) - P_0(\cdot)\|_{C^1} \to 0, \quad \tau \to 0.$$

Thus, it suffice to take τ small enough to ensure the neighborhood condition (5.12).

Step 3: Contraction mapping In order to verify (5.13), we let $\begin{pmatrix}\tilde{w}\\ \tilde{P}\end{pmatrix}, \begin{pmatrix}w\\ P\end{pmatrix} \in \overline{B_{\tilde{Z}^\tau}}\left(\begin{pmatrix}w^0\\ P^0\end{pmatrix}, r\right)$. We observe that

$$\begin{aligned}\left|\tilde{w}^1(t,x)-w^1(t,x)\right| &= \Big|u_0(x)\exp\Big(\int_0^t F(w(l,x))+P(l,\Pi(l,0;x))\mathrm{d}l\Big)\\ &\quad - u_0(x)\exp\Big(\int_0^t F(\tilde{w}(l,x))+\tilde{P}(l,\tilde{\Pi}(l,0;x))\mathrm{d}l\Big)\Big|.\end{aligned}$$

Due to the classical inequality $|e^x-e^y|\le e^{x+y}|x-y|$ which holds for any $x, y\in\mathbb{R}$, we deduce

$$\begin{aligned}&\left|\tilde{w}^1(t,x)-w^1(t,x)\right|\\ &\le \|u_0\|_{C^0}e^{2\tau(\tilde{F}+\kappa)}\Big[\int_0^t \|F(\tilde{w}(l,\cdot))-F(w(l,\cdot))\|_{C^0}\mathrm{d}l\\ &\quad+\int_0^t \|\tilde{P}(l,\tilde{\Pi}(l,0;\cdot))-P(l,\Pi(l,0;\cdot))\|_{C^0}\mathrm{d}l\Big]\\ &\le \|u_0\|_{C^0}e^{2\tau(\tilde{F}+\kappa)}\Big[\tau\tilde{F}\sup_{l\in[0,\tau]}\|\tilde{w}(l,\cdot)-w(l,\cdot)\|_{C^0}\\ &\quad+\tau\sup_{l\in[0,\tau]}\|\tilde{P}(l,\tilde{\Pi}(l,0;\cdot))-P(l,\tilde{\Pi}(l,0;\cdot))\|_{C^0}\\ &\quad+\tau\sup_{l\in[0,\tau]}\|P(l,\tilde{\Pi}(l,0;\cdot))-P(l,\Pi(l,0;\cdot))\|_{C^0}\Big]\\ &\le \|u_0\|_{C^0}e^{2\tau(\tilde{F}+\kappa)}\Big[\tau\tilde{F}\sup_{l\in[0,\tau]}\|\tilde{w}(l,\cdot)-w(l,\cdot)\|_{C^0}+\tau\sup_{l\in[0,\tau]}\|\tilde{P}(l,\cdot)-P(l,\cdot)\|_{C^0}\\ &\quad+\tau\sup_{l\in[0,\tau]}\|P(l,\cdot)\|_{W^{1,\infty}}\sup_{l\in[0,\tau]}\|\tilde{\Pi}(l,0;\cdot)-\Pi(l,0;\cdot)\|_{C^0}\Big]\\ &\le \tau\|u_0\|_{C^0}e^{2\tau(\tilde{F}+\kappa)}\Big[\tilde{F}\|\tilde{w}-w\|_{X^\tau}+\|\tilde{P}-P\|_{Y^\tau}\\ &\quad+C_2\sup_{l\in[0,\tau]}\|\tilde{\Pi}(l,0;\cdot)-\Pi(l,0;\cdot)\|_{C^0}\Big].\end{aligned}\tag{5.20}$$

To estimate $\sup_{l\in[0,\tau]}\|\tilde{\Pi}(l,0;\cdot)-\Pi(l,0;\cdot)\|_{C^0}$ in (5.20), we claim that

$$\sup_{t,s\in[0,\tau]}\|\tilde{\Pi}(t,s;\cdot)-\Pi(t,s;\cdot)\|_{C^0}\le\tau e^{\tau C_2}\sup_{t\in[0,\tau]}\|\tilde{P}(l,\cdot)-P(l,\cdot)\|_{C^1}\tag{5.21}$$

Indeed, we can obtain that

$$\left|\tilde{\Pi}(t,s;x)-\Pi(t,s;x)\right|=\left|\int_s^t\nabla\tilde{P}(l,\tilde{\Pi}(l,s;x))-\nabla P(l,\Pi(l,s;x))\mathrm{d}l\right|$$

$$
\begin{aligned}
&\le \int_s^t \|\nabla \tilde{P}(l, \tilde{\Pi}(l,s;\cdot)) - \nabla P(l, \tilde{\Pi}(l,s;\cdot))\|_{C^0} \mathrm{d}l \\
&\quad + \int_s^t \|\nabla P(l, \tilde{\Pi}(l,s;\cdot)) - \nabla P(l, \Pi(l,s;\cdot))\|_{C^0} \mathrm{d}l \\
&\le \tau \sup_{l\in[0,\tau]} \|\nabla \tilde{P}(l, \tilde{\Pi}(l,s;\cdot)) - \nabla P(l, \tilde{\Pi}(l,s;\cdot))\|_{C^0} \\
&\quad + \sup_{l\in[0,\tau]} \|\nabla P(l,\cdot)\|_{W^{1,\infty}} \int_s^t \|\tilde{\Pi}(l,s;\cdot) - \Pi(l,s;\cdot)\|_{C^0} \mathrm{d}l.
\end{aligned}
$$

This leads to

$$
\begin{aligned}
\sup_{t,s\in[0,\tau]} \|\tilde{\Pi}(t,s;\cdot) - \Pi(t,s;\cdot)\|_{C^0} &\le \tau \sup_{l\in[0,\tau]} \|\tilde{P}(l,\cdot) - P(l,\cdot)\|_{C^1} \\
&\quad + C_2 \int_s^t \|\tilde{\Pi}(l,s;\cdot) - \Pi(l,s;\cdot)\|_{C^0} \mathrm{d}l.
\end{aligned}
$$

Again due to Grönwall's inequality, we conclude that (5.21) holds.

Inserting (5.21) into (5.20) we have

$$
\begin{aligned}
&\sup_{t\in[0,\tau]} \left\| \tilde{w}^1(t,\cdot) - w^1(t,\cdot) \right\|_{C^0} \\
&\quad \le \|u_0\|_{C^0} e^{2\tau(\tilde{F}+\kappa)} \Big[\tau \tilde{F} \|\tilde{w} - w\|_{X^\tau} + \tau \|\tilde{P} - P\|_{Y^\tau} + \tau^2 C_2 \, e^{\tau C_2} \|\tilde{P} - P\|_{Y^\tau} \Big] \\
&\quad \le \tau \|u_0\|_{C^0} e^{2\tau(\tilde{F}+\kappa)} \Big[\tilde{F} \|\tilde{w} - w\|_{X^\tau} + \Big(1 + \tau \, C_2 \, e^{\tau C_2}\Big) \|\tilde{P} - P\|_{Y^\tau} \Big] \\
&\quad \le L_1(\tau) \Big[\|\tilde{w} - w\|_{X^\tau} + \|\tilde{P} - P\|_{Y^\tau} \Big],
\end{aligned} \tag{5.22}
$$

where we set

$$
L_1(\tau) := \tau \|u_0\|_{C^0} e^{2\tau(\tilde{F}+\kappa)} \Big(\tilde{F} + \Big(1 + \tau \, C_2 \, e^{\tau C_2}\Big) \Big)
$$

and $L_1(\tau) \to 0$ as $\tau \to 0$.

Next we prove the contraction property for $\|\tilde{P}^1 - P^1\|_{Y^\tau}$. As before, applying the same argument of Morrey's inequality and the classical elliptic estimates, we can deduce

$$
\begin{aligned}
\|\tilde{P}^1(t,\cdot) - P^1(t,\cdot)\|_{C^1} &\le C \|\tilde{w}^1(t, \tilde{\Pi}(0,t;\cdot)) - w^1(t, \Pi(0,t;\cdot))\|_{L^4} \\
&\le C \|\tilde{w}^1(t, \tilde{\Pi}(0,t;\cdot)) - w^1(t, \Pi(0,t;\cdot))\|_{C^0} \\
&\le C \|\tilde{w}^1(t, \tilde{\Pi}(0,t;\cdot)) - w^1(t, \tilde{\Pi}(0,t;\cdot))\|_{C^0} \\
&\quad + C \|w^1(t, \tilde{\Pi}(0,t;\cdot)) - w^1(t, \Pi(0,t;\cdot))\|_{C^0} \\
&\le C \|\tilde{w}^1(t,\cdot) - w^1(t,\cdot)\|_{C^0} \\
&\quad + C \|w^1\|_{W^{1,\infty}} \|\tilde{\Pi}(0,t;\cdot) - \Pi(0,t;\cdot)\|_{C^0}
\end{aligned}
$$

$$
\begin{aligned}
&\leq C\|\tilde{w}^1(t,\cdot)-w^1(t,\cdot)\|_{C^0}\\
&\quad + C\ C_1\|\tilde{\Pi}(0,t;\cdot)-\Pi(0,t;\cdot)\|_{C^0}\\
&\leq C\|\tilde{w}^1(t,\cdot)-w^1(t,\cdot)\|_{C^0}\\
&\quad + C\ C_1\ \tau\ e^{\tau C_2}\ \sup_{t\in[0,\tau]}\|\tilde{P}(t,\cdot)-P(t,\cdot)\|_{C^1},
\end{aligned}
$$

where we used (5.21) in the last inequality and C is a constant depending only on Ω. Defining $L_2(\tau) := C\ C_1\ \tau\ e^{\tau C_2}$ and together with (5.22) we obtain

$$
\sup_{t\in[0,\tau]}\|\tilde{P}^1(t,\cdot)-P^1(t,\cdot)\|_{C^1} \leq C\ L_1(\tau)\Big[\|\tilde{w}-w\|_{X^\tau}+\|\tilde{P}-P\|_{Y^\tau}\Big]+L_2(\tau)\|\tilde{P}-P\|_{Y^\tau}. \tag{5.23}
$$

Combing with (5.22) and (5.23) we deduce

$$
\|\tilde{w}^1-w^1\|_{X^\tau}+\|\tilde{P}^1-P^1\|_{Y^\tau} \leq \big(C\ L_1(\tau)+L_2(\tau)\big)\Big[\|\tilde{w}-w\|_{X^\tau}+\|\tilde{P}-P\|_{Y^\tau}\Big], \tag{5.24}
$$

where $L_i(\tau)\to 0,\ i=1,2$ as $\tau\to 0$. If τ is small enough, this implies (5.13) for some $\theta\in(0,1)$. Since $\tilde{Z}^\tau$ is complete metric space for the distance induced by the norm $(\|\cdot\|_{X^\tau},\|\cdot\|_{Y^\tau})$ in Z_τ, the result follows by the classical Banach fixed point theorem. □

Remark 5.6 Let us mention that we can derive a maximal time of solutions as long as the $W^{1,\infty}(\Omega)$ norm of $u(t,.)$ stays bounded. This can be seen by using our local existence result together with the following observations. Let $t_0>0$ and assume that the solution exists until $t=t_0$. We define for all $t,s\geq t_0$

$$
\begin{cases}
\frac{\partial}{\partial t}\Pi_{t_0}(t,s;x) = -d\,\nabla P(t+t_0,\Pi_{t_0}(t,s;x)),\\
\Pi_{t_0}(s,s;x) = x\in\Omega.
\end{cases} \tag{5.25}
$$

Then by the uniqueness of solutions we deduce that

$$
\Pi_{t_0}(t,s;x) = \Pi(t+t_0,s+t_0;x)
$$

where Π is the solution of (2.4). Moreover

$$
w(t+t_0,x) := u(t+t_0,\Pi(t+t_0,0;x)) = u(t+t_0,\Pi(t+t_0,t_0;\Pi(t_0,0;x)).
$$

Choose $x=\Pi(t_0,0;\widehat{x})$ then in order to deal the fixed point problem starting t_0 it is natural to introduce

$$
w_{t_0}(t,\widehat{x}) := w(t+t_0,\Pi(0,t_0;x)) = u(t+t_0,\Pi_{t_0}(t,0;\widehat{x})). \tag{5.26}
$$

By combining Eqs. (5.25)–(5.26), we can deduce the existence and uniqueness of solutions as long as the $W^{1,\infty}(\Omega)$ norm of $u(t,.)$ is bounded. This idea can be used to derive a maximal semiflow in the sense (Magal and Ruan 2018, Chapter 5).

5.3 Parameter fitting

From the work in Pasquier et al. (2011), MCF-7 and MCF-7/Doxo cells are cultured at 10^5 initial number of cells separately in 60×15 mm cell Petri dish with or without doxorubicine. We use the cell proliferation data followed every 12 h during 6 days to fit the parameters of the following ordinary differential equation

$$\begin{cases} \dfrac{du_i}{dt} = u_i(b_i - a_{ii}u_i) - \delta_i u_i \quad i = 1, 2. \\ u_i(0) = u_{i,0}. \end{cases} \tag{5.27}$$

Here we use u_1 to represent the MCF-7 (sensitive to drug) and u_2 to represent the MCF-7/Doxo (resistant to drug) and $b_i > 0$ is the growth rate δ_i is the extra mortality rate caused by drug (doxorubicine) treatment and $a_{ii} > 0$ is a coefficient which controls the carrying capacity.

In the work Sutherland et al. (1983) cell proliferation kinetics for MCF-7 is studied over 11 days in 150 cm^2 flask. Following an inoculation of 3×10^5 cells at day 0, a maximum cell density of 8–9 $\times 10^7$ cells/flask was reached at day 11. Therefore, we assume the carrying capacity for each species in 60×15 mm (surface of 21.5 cm^2) Petri dish satisfies

$$\frac{b_i}{a_{ii}} \approx 9 \times 10^7 \times \frac{21.5\,\text{cm}^2}{150\,\text{cm}^2} = 1.29 \times 10^7, \quad i = 1, 2.$$

By fixing the carrying capacity, we first estimate the growth rate b_i of each species under zero drug concentration, namely $\delta_i = 0$. We divide the number of cells by $u_{i,0} = 10^5$ (the initial number of cells) and rescale the parameters as follows

$$\tilde{u}_i = \frac{u_i}{10^5}, \quad \tilde{a}_i = a_{ii} \times 10^5, \quad \tilde{b}_i = b_i. \tag{5.28}$$

As seen in Fig. 23, without treatment, MCF-7 and MCF-7/Doxo displayed very similar growth rates, 0.6420 and 0.6359 per day, respectively.

By fixing the parameters

$$b_1 = 0.6420,\ a_{11} = 0.0050, \quad b_2 = 0.6359,\ a_{22} = 0.0049, \tag{5.29}$$

we consider different scenarios with the drug concentration varies from 0.1 to 10 μM (see Fig. 24) and we estimate the extra mortality rate δ_i for each population due to doxorubicine (see Table 4).

5.4 Numerical scheme

For simplicity, we give the numerical scheme for the following one species and one dimensional model

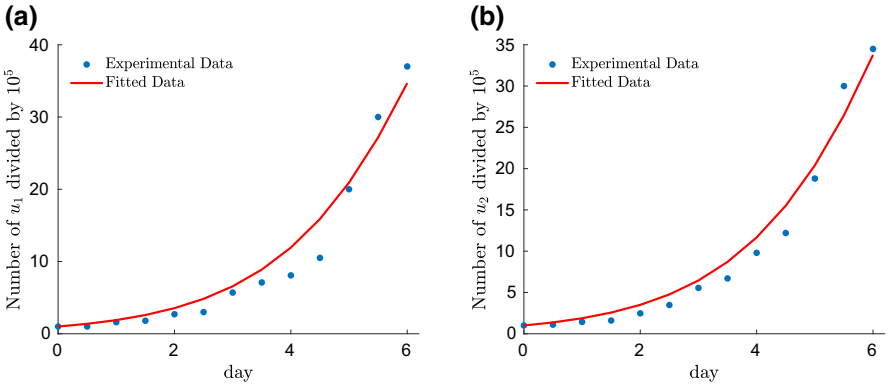

Fig. 23 Fitting for the parameters (under rescaling (5.28)) in model (5.27). We plot the experimental data (dots in **a**) of MCF-7 (sensitive to drug) and (dots in **b**) MCF-7/Doxo (resistant to drug) with no drug concentration over 6 days. We obtain an estimation of the growth rates $b_1 = 0.6420, b_2 = 0.6359$ and $a_{11} = 0.0050, a_{22} = 0.0049$

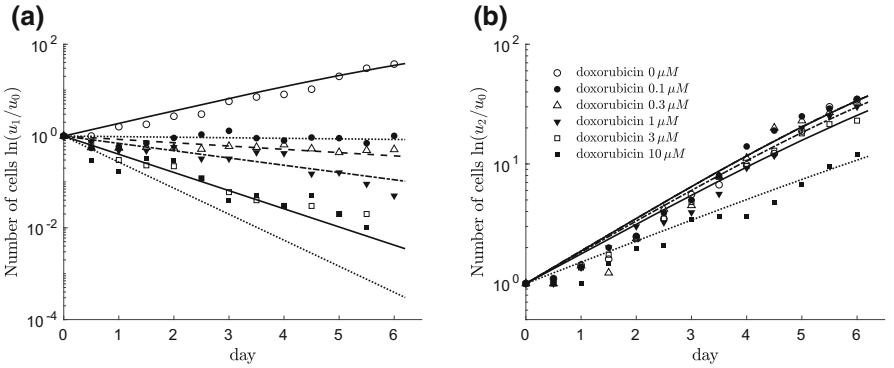

Fig. 24 Fitting for the growth curves of MCF-7 (**a**) and MCF-7/Doxo (**b**) under different drug concentrations in model (5.27) over 6 days. Cells were grown in the absence or presence of doxorubicine (0.1–10 μM, corresponding symbols given in the legend in **b**) and counted every 12 h in a Malassez chamber. Cell counts are expressed as the logarithm of the numbers of cells (u_i) divided by the number of cells at day 0 ($u_{i,0}$). We fix the growth rate b_i and a_{ii}, $i = 1, 2$ as in (5.29)

Table 4 List of the estimation of extra mortality rate δ_1 for the sensitive cell and δ_2 for the resistant cell under different concentrations of doxorubicine

Drug concentration (μM)	0	0.1	0.3	1	3	10
Extra mortality δ_1 (day^{-1})	0	0.6619	0.8109	1.0118	1.5585	1.9545
Extra mortality δ_2 (day^{-1})	0	0	0	0.0246	0.0569	0.2192

$$\begin{cases} \partial_t u + d\,\partial_x\,(u\partial_x P) = f(u) & \text{in } (0,T]\times[-L,L] \\ (I-\chi\Delta)P(t,x) = u(t,x) & \\ \partial_x P(t,\pm L) = 0 & \text{on } [0,T]. \end{cases} \tag{5.30}$$

The numerical method used is based on finite volume method. We refer to Leveque (2002) and Toro (2013) for more results about this subject. Our numerical scheme reads as follows

$$u_i^{n+1} = u_i^n - d\,\frac{\Delta t}{\Delta x}\Big(\phi(u_{i+1}^n, u_i^n) - \phi(u_i^n, u_{i-1}^n)\Big) + \Delta t\, f(u_i^n), \quad i = 1, 2, \ldots, M,\ n = 0, 1, 2, \ldots, N, \tag{5.31}$$

with the flux $\phi(u_{i+1}^n, u_i^n)$ defined as

$$\phi\left(u_{i+1}^n, u_i^n\right) = \left(v_{i+\frac{1}{2}}^n\right)^+ u_i^n - \left(v_{i+\frac{1}{2}}^n\right)^- u_{i+1}^n = \begin{cases} v_{i+\frac{1}{2}}^n u_i^n, & v_{i+\frac{1}{2}}^n \geq 0, \\ v_{i+\frac{1}{2}}^n u_{i+1}^n, & v_{i+\frac{1}{2}}^n < 0. \end{cases} \tag{5.32}$$

and

$$v_{i+\frac{1}{2}}^n = -\frac{l_{i+1}^n - l_i^n}{\Delta x}, \quad i = 0, 1, 2, \ldots, M, \tag{5.33}$$

where we define

$$L^n := (I - \chi A)^{-1} U^n, \quad n = 0, 1, 2, \ldots, N, \quad L_i^n = \left(l_i^n\right)_{M\times 1} \quad U^n = \left(u_i^n\right)_{M\times 1}.$$

where χ is a constant and $A = (a_{i,j})_{M\times M}$ is the usual linear diffusion matrix with Neumann boundary condition. Therefore, since the Neumann boundary condition corresponds to a no flux boundary condition, we impose

$$\begin{aligned} \phi\left(u_1^n, u_0^n\right) &= 0, \\ \phi\left(u_{M+1}^n, u_M^n\right) &= 0. \end{aligned} \tag{5.34}$$

which corresponds to $l_0 = l_1$ and $l_{M+1} = l_M$.

The numerical scheme at the boundary becomes

$$\begin{aligned} u_1^{n+1} &= u_1^n - d\,\frac{\Delta t}{\Delta x}\phi(u_2^n, u_1^n) + \Delta t\, f(u_1^n), \\ u_M^{n+1} &= u_M^n + d\,\frac{\Delta t}{\Delta x}\phi(u_M^n, u_{M-1}^n) + \Delta t\, f(u_M^n). \end{aligned}$$

By this boundary condition, we have the conservation of mass for Eq. (5.30) when the reaction term $f \equiv 0$.

References

Ambrosio L (2000) Geometric evolution problems, distance function and viscosity solutions. In: Ambrosio L, Dancer N (eds) Calculus of variations and partial differential equations. Springer, Berlin, pp 5–93

Armstrong NJ, Painter KJ, Sherratt JA (2006) A continuum approach to modelling cell–cell adhesion. J Theor Biol 243:98–113

Bailey PC, Lee RM, Vitolo MI, Pratt SJ, Ory E, Chakrabarti K, Lee CJ, Thompson KN, Martin SS (2018) Single-cell tracking of breast cancer cells enables prediction of sphere formation from early cell divisions. iScience 8:29–39

Bellomo N, Bellouquid A, Nieto J, Soler J (2012) On the asymptotic theory from microscopic to macroscopic growing tissue models: an overview with perspectives. Math Models Methods Appl Sci 22(01):1130001

Bertsch M, Hilhorst D, Izuhara H, Mimura M (2012) A nonlinear parabolic–hyperbolic system for contact inhibition of cell-growth. Differ Equ Appl 4:137–157

Burger M, Fetecau R, Huang Y (2014) Stationary states and asymptotic behavior of aggregation models with nonlinear local repulsion. SIAM J Appl Dyn Syst 13(1):397–424

Calvez V, Dolak-Struß Y (2008) Asymptotic behavior of a two-dimensional Keller–Segel model with and without density control. Math Model Biol Syst 2:323–337

Carrillo JA, Murakawa H, Sato M, Togashi H, Trush O (2019) A population dynamics model of cell–cell adhesion incorporating population pressure and density saturation. J Theor Biol 474:14–24

Conti M, Terracini S, Verzini G (2005) A variational problem for the spatial segregation of reaction–diffusion systems. Indiana Univ Math J 54(3):779–815

Crooks EC, Dancer EN, Hilhorst D, Mimura M, Ninomiya H (2004) Spatial segregation limit of a competition–diffusion system with Dirichlet boundary conditions. Nonlinear Anal Real World Appl 5(4):645–665

Dancer EN, Hilhorst D, Mimura M, Peletier LA (1999) Spatial segregation limit of a competition–diffusion system. Eur J Appl Math 10(2):97–115

Ducrot A, Magal P (2014) Asymptotic behavior of a nonlocal diffusive logistic equation. SIAM J Math Anal 46(3):1731–1753

Ducrot A, Fu X, Magal P (2018) Turing and Turing–Hopf bifurcations for a reaction diffusion equation with nonlocal advection. J Nonlinear Sci 28(5):1959–1997

Dyson J, Gourley SA, Villella-Bressan R, Webb GF (2010) Existence and asymptotic properties of solutions of a nonlocal evolution equation modeling cell–cell adhesion. SIAM J Math Anal 42(4):1784–1804

Eftimie R, de Vries G, Lewis MA, Lutscher F (2007) Modeling group formation and activity patterns in self-organizing collectives of individuals. Bull Math Biol 69:1537–1565

Evans LC (1998) Partial differential equations. American Mathematical Society, Providence

Foote RL (1984) Regularity of the distance function. Proc Am Math Soc 92(1):153–155

Fu X (2019) Reaction–diffusion equations with nonlinear and nonlocal advection applied to cell co-culture. Doctoral dissertation

Fu X, Magal P (2018) Asymptotic behavior of a nonlocal advection system with two populations. arXiv preprint arXiv:1812.06733

Gilbarg D, Trudinger NS (2001) Elliptic partial differential equations of second order. Classics in mathematics. U.S. Government Printing Office, Washington

Hillen T, Painter KJ (2009) A user's guide to PDE models for chemotaxis. J Math Biol 58(1–2):183–217

Hirsch MW, Smale S, Devaney RL (2012) Differential equations, dynamical systems, and an introduction to chaos. Academic Press, Cambridge

Horstmann D (2003) From 1970 until present: the Keller–Segel model in chemotaxis and its consequences. J Jahresber DMV 105(3):103–165

Katsunuma S, Honda H, Shinoda T, Ishimoto Y, Miyata T, Kiyonari H, Abe T, Nibu K, Takai Y, Togashi H (2016) Synergistic action of nectins and cadherins generates the mosaic cellular pattern of the olfactory epithelium. J Cell Biol 212(5):561–575

Keller EF, Segel LA (1971) Model for chemotaxis. J Theor Biol 30:225–234

Leveque RJ (2002) Finite volume methods for hyperbolic problems. Cambridge University Press, Cambridge

Leverentz AJ, Topaz CM, Bernoff AJ (2009) Asymptotic dynamics of attractive–repulsive swarms. SIAM J Appl Dyn Syst 8(3):880–908

Lou Y, Ni WM (1996) Diffusion, self-diffusion and cross-diffusion. J Differ Equ 131(1):79–131

Magal P, Ruan S (2018) Theory and applications of abstract semilinear Cauchy problems, vol 201. Springer, Berlin

Mimura M, Kawasaki K (1980) Spatial segregation in competitive interaction–diffusion equations. J Math Biol 9(1):49–64

Mimura M, Nishiura Y, Tesei A, Tsujikawa T (1984) Coexistence problem for two competing species models with density-dependent diffusion. Hiroshima Math J 14(2):425–449

Mogilner A, Edelstein-Keshet L, Bent L, Spiros A (2003) Mutual interactions, potentials, and individual distance in a social aggregation. J Math Biol 47:353–389
Morale D, Capasso V, Oelschläger K (2005) An interacting particle system modelling aggregation behavior: from individuals to populations. J Math Biol 50:49–66
Murakawa H, Togashi H (2015) Continuous models for cell–cell adhesion. J Theor Biol 372:1–12
Murray JD (2003) Mathematical biology I: an introduction, vol I. Springer, Berlin
Ni W, Shi J, Wang M (2018) Global stability and pattern formation in a nonlocal diffusive Lotka–Volterra competition model. J Differ Equ 264(11):6891–6932
Pasquier J, Magal P, Boulangé-Lecomte C, Webb GF, Le Foll F (2011) Consequences of cell-to-cell P-glycoprotein transfer on acquired multi-drug resistance in breast cancer: a cell population dynamics model. Biol Direct 6(1):5
Pasquier J, Galas L, Boulangé-Lecomte C, Rioult D, Bultelle F, Magal P, Webb G, Le Foll F (2012) Different modalities of intercellular membrane exchanges mediate cell-to-cell P-glycoprotein transfers in MCF-7 breast cancer cells. J Biol Chem 287(10):7374–7387
Patlak CS (1953) Random walk with persistence and external bias. Bull Math Biophys 15:311–338
Perthame B, Dalibard AL (2009) Existence of solutions of the hyperbolic Keller–Segel model. Trans Am Math Soc 361(5):2319–2335
Shi J, Wang C, Wang H (2019a) Diffusive spatial movement with memory and maturation delays. Nonlinearity 32(9):3188–3208
Shi J, Wang C, Wang H, Yan X (2019b) Diffusive spatial movement with memory. J Dyn Differ Equ. https://doi.org/10.1088/1361-6544/ab1f2f
Shigesada N, Kawasaki K, Teramoto E (1979) Spatial segregation of interacting species. J Theor Biol 79(1):83–99
Song Y, Wu S, Wang H (2019) Spatiotemporal dynamics in the single population model with memory-based diffusion and nonlocal effect. J Differ Equ 267:6316–6351
Sutherland RL, Hall RE, Taylor IW (1983) Cell proliferation kinetics of MCF-7 human mammary carcinoma cells in culture and effects of tamoxifen on exponentially growing and plateau-phase cells. Cancer Res 43(9):3998–4006
Taylor HB, Khuong A, Wu Z, Xu Q, Morley R, Gregory L, Poliakov A, Taylor WR, Wilkinson DG (2017) Cell segregation and border sharpening by Eph receptor-ephrin-mediated heterotypic repulsion. J R Soc Interface 14(132):20170338
Toro EF (2013) Riemann solvers and numerical methods for fluid dynamics: a practical introduction. Springer, Berlin
Zeeman ML (1995) Extinction in competitive Lotka–Volterra systems. Proc Am Math Soc 123(1):87–96